University of Cincinnati

Date: 6/3/2011

I, Rajiv Krishnan Venkatakrishnan , hereby submit this original work as part of the requirements for the degree of Master of Science in Electrical Engineering.

It is entitled:

Compact Metamaterial UHF RFID Tag Antennas

Student's name: **Rajiv Krishnan Venkatakrishnan**

This work and its defense approved by:

Committee chair: Altan Ferendeci, PhD

Committee member: Joseph Thomas Boyd, PhD

Committee member: Carla Purdy, C, PhD

1875

Compact Metamaterial UHF RFID Tag Antennas

A thesis submitted to the

Graduate School of University of Cincinnati

In partial fulfillment of the requirements for the degree of

MASTER OF SCIENCE

In the Department of Electrical Engineering

Of the College of Engineering

June 2011

By

Rajiv Krishnan Venkatakrishnan

B.E. Electronics and Communication Engineering

Madras University

May 2004

Thesis Advisor and Committee Chair: Dr. Altan M. Ferendeci

Abstract

The unusual properties exhibited by left-handed metamaterials have been of great interest to researchers, especially in the field of RF and Microwave communication. The property of backward-wave propagation has led to a number of applications which were not possible with natural right-handed materials. One of the most exciting applications of these left-handed metamaterials is the Zeroth Order Resonator (ZOR) wherein resonance is achieved even at the zeroth mode, which is not possible with the traditional right-handed materials. This has led to the design of Composite Right/Left-Handed (CRLH) ZOR antennas whose resonance frequency does not depend on the physical length of the resonator.

In this thesis the theory behind the ZOR antennas is studied and their applicability for use as RFID tag antennas is explored. Three novel CRLH ZOR antenna configurations are proposed targeting the UHF RFID tag application. The antennas are simulated using Agilent ADS Momentum and the simulation results are compared with those of the traditional 2-cell and 4-cell CRLH ZOR antennas that have been previously designed. The novel antennas are also compared with a simple rectangular patch antenna to demonstrate the reduction in size achieved through the use of left-handed metamaterials. The novel antennas are also simulated with varying values of the substrate height, metal thickness, and dielectric loss tangent and the effect of these parameters on antenna performance is analyzed. The three novel antennas and a rectangular patch antenna are fabricated and the experimental results are presented. The novel antennas are found to be around 30 times smaller than the rectangular patch antenna radiating at the same frequency.

Acknowledgements

It is my foremost duty to thank my advisor Dr. Altan M. Ferendeci who introduced me to the field of Radio Frequency and whose constant support and guidance made this work possible. I would also like to thank Dr. Carla C. Purdy and Dr. Joseph T. Boyd for graciously accepting to be a part of my thesis defense committee.

The people I have missed the most during the period of my Masters are my parents and my sister. Their constant encouragement and moral support has helped me get through the toughest of times. This thesis is dedicated to the unconditional love that they have showered on me.

I have to thank my wonderful friends Chandrika, Hema, Surya, Devi, Sanu, and Prasanna, who brightened up the last two years of my life in Cincinnati. I am eternally grateful to Chandrika and Hema for their constant words of encouragement that has helped me stay positive even through periods of despair. I would also like to thank my other friends in Cincinnati and my buddies around the world for all the encouragement and support.

I would finally like to thank the almighty for making this experience possible.

'*Sri Gurubhyo Namaha*'

Table of Contents

List of Figures

List of Tables

Chapter 1

Introduction

1.1 The World of RFID

Radio Frequency Identification (RFID) is an emerging technology that is increasingly being used in all sectors. Some of the most prevalent applications of RFID lie in the retail sector with the mandate issued by Wal-Mart acting as the major reason for most manufacturers to implement RFID [1]. The technical advantages of RFID over other identification technologies such as Bar Codes have been well documented. The RFID implementation has been profitable for some manufacturers while it has been a burden for others. This is because RFID proves to be a profitable option only when used throughout the manufacturing cycle.

RFID systems essentially consist of a Tag and a Reader. The tag is a simple system that consists of a RFID chip attached to an antenna. The Reader is a much more complicated system and is essentially a transceiver system which has to both transmit signals to the tag and receive the tag's response. RFID tags can be classified based on their mode of operation and by their operating frequency band [1].

Mode of Operation

- Passive Tag – The tag does not have a battery and the power required to drive the chip is derived from the signal sent by the reader.
- Semi-Passive Tag - The tag has a battery on-board which is used only to drive the chip and not to send a signal.

- Active Tag – The tag has a battery which is used both to drive the chip as well as to beacon signals to the reader.

Frequency of Operation

- Low Frequency Tags (LF) – Operate between 125-134 kHz and use near-field inductive coupling for power and communication.
- High Frequency Tags (HF) – Operate at 13.56 MHz and also use near-field inductive coupling for power and communication.
- Ultra-High Frequency Tags (UHF) – Passive tags operate between 860-960 MHz (exact band used varies in different countries) while active tags operate at 433 MHz.
- Microwave Tags – Operate either at 2.4 GHz or 5.8 GHz.

This thesis deals with the *Passive UHF RFID* tag, specifically the design of a novel tag antenna based on metamaterials.

1.2 Antennas in RFID

Antennas are the heart of any RFID system. Poor antenna design could play a major role in compromising the performance of the whole system. The primary characteristics to be considered when designing a RFID Tag antenna are the size, the read range, and the manufacturing cost of the antenna. The ideal tag antenna would have a really small form factor, a high read range, and also be manufactured at a very low cost. However as in most cases the ideal scenario is not feasible because when any two of the above conditions are met the third condition tends to fail. Hence the idea behind a tag antenna design is the management of the trade-off

between these three conditions. A comprehensive review of the design considerations for a tag antenna is given in [2].

Most antennas currently used in passive RFID applications are printed antennas with no ground planes, which have a very small form factor and can be manufactured at a very low cost although their read range is not very high. As mentioned in [2], various other novel antenna designs have been proposed such as Slotted antenna [3], Circular patch antenna [4], Meander Line antenna [5], Inverted-F antenna [6], and Folded Dipole antenna [7].

The simple rectangular patch antenna has also been tested for working as a RFID Tag [8]. Although the patch is found to provide a good performance with respect to read range and cost, it cannot be used in practical applications due to its large form factor. The antenna designed in this thesis aims to provide a similar performance to the simple patch but with much smaller form factor.

1.3 RFID Tag Antenna Metal-Water Problem

A major problem impeding the growth of passive RFID systems is the poor performance of RF antennas when either metals or liquids are in close proximity [9][10][11]. Under these conditions the read range is found to decrease sharply and is attributed to decrease in the electric field near the surface which is required to meet the boundary conditions. When the tag is close to the object; antenna detuning plays an important role [12]. The link budget analysis in [13] shows an 18dB loss when the tag is placed onto lossy and metallic surfaces.

There have been various attempts made to solve the metal surface problem. The most common solution has involved the use of a spacer in order to separate the tag from the metal on which it has been affixed. The other solution has been to use a special tag designed specifically for use

with metals which provides a really good performance but with a considerable cost overhead. The solution that would be desirable is a tag which works on all materials without a significant performance degradation when used with metals.

Ng et al have demonstrated the use of the simple rectangular patch antenna tag as a solution to this problem [8]. The concept behind the use of a patch antenna on metallic objects is the presence of a metallic ground plane which is part of the antenna design. When the patch antenna is affixed onto a metallic object it just acts as an extension of the ground plane which in fact could lead to an improvement in performance [14]. However, as mentioned in the previous section, the limiting factor of this design is the large size of the patch which precludes its use in real-life applications. An antenna with a ground plane which also has a small form factor, such as the antenna designed in this thesis, would be a good solution for the metal surface problem.

1.4 Motivation and Related Research

Metamaterials and RFID are both topics that have been extensively researched. The origin of research on Metamaterials dates back to the paper written by Viktor Veselago in 1967 [15]. Though Veselago theorized the concept of Metamaterials, it took a long time before it was actually verified experimentally [16]. The book by Caloz and Itoh [17] completely describes all the research that has been done on Metamaterials. Chapter 3 of this thesis delves deeper into the concept of Metamaterials.

The inspiration behind the antenna designed in this thesis is the work done by Bo Zhao [18]. Zhao has designed a Composite Right/Left Handed (CRLH) Zeroth Order Resonant (ZOR) antenna which radiates at 2.4 GHz and excellent performance is shown through simulations done using Advanced Design System (ADS). This thesis uses the same approach to design a CRLH-

ZOR antenna radiating at 915 MHz and the results are displayed using ADS simulations. The simulation results are also verified experimentally by testing the antenna in an anechoic chamber. The drawback in [18] is that the simulations have been performed assuming a perfect conductor which is an ideal case not attainable in practice. The simulations done in this thesis incorporates Copper conductivity for real performance of the antennas.

As mentioned earlier, the proof of concept work done by Ng et al [8] is used to design the antennas in this thesis as RFID tag antennas with the goal of using these antennas within the metallic environment. A patch antenna as a UHF RFID tag is also designed and tested.

1.5 Thesis Organization

This chapter has given a brief introduction to the concept of RFID. The antennas used in RFID were described. The motivation behind the research done in this thesis was outlined and a short overview of the related research performed in this area was provided.

Chapter 2 gives a detailed description of Antennas and the various parameters involved. It delves into the different types of antennas and some of the important testing parameters used in this thesis. A section is dedicated to Microstrip antenna design which is the base concept for the CRLH antenna.

The concept of Metamaterials is elucidated in *Chapter 3*. The CRLH theory and the Zeroth Order Resonator (ZOR) design are explained in detail. *Chapter 4* details the design of the novel ZOR antenna and presents the simulated and experimental results. It also provides a performance comparison with the traditional 2-cell and 4-cell CRLH ZOR antennas. A size comparison of the novel antennas with the standard rectangular patch antenna is also shown. The conclusions and recommendations for future work are provided in *Chapter 5*.

Chapter 2

Fundamentals of Antennas

2.1 Introduction

Antennas are the most important aspect of any communication system. They enable the transmission and reception of Electromagnetic waves without which a communication system would be rendered useless. The basic principle on which all antennas function is the electromagnetic theory formulated by James Maxwell in 1873 [19]. It took 13 years for Maxwell's theory to be validated, when Heinrich Hertz created the first ever radio system which used a dipole transmitting antenna and a resonant loop receiving antenna [20]. Long distance communication was first achieved by Marconi in 1901 when he successfully sent signals across the Atlantic using a fan antenna. The paper by Kraus [21] and the book by Silver [22] describe some of the initial antennas which were designed.

Antennas have applications in almost every area such as Radio, TV, Wireless Communication, astronomy, radar, air traffic control, etc. A detailed description of the various antenna applications at various frequencies and their impact on systems is provided in [23]. The application that this thesis is concerned about is RFID where antennas play a major role in both the tag and the reader systems.

The electrical and mechanical parameters of antennas determine their suitability to any application. The operating frequency, directivity, antenna gain, radiation efficiency, impedance, etc. are some of the electrical parameters. Some of the important mechanical parameters include

the form factor, thickness, weight, and the dielectric material used. The parameters of interest are explained in further detail later in this chapter.

2.2 Classification of Antennas

There are a variety of antenna designs currently in existence which may be broadly classified by their operating frequency band or their basic operating mode. Based on the mode of operation [24] defines four groups of antennas: *elemental electric and magnetic currents*, *travelling-wave antennas*, *array antennas* and *radiating aperture antennas*. This classification is only approximate as there could be a number of antennas which might not fall under any single category. A more general classification provided by [25] classifies antennas into four types: *electrically small antennas*, *resonant antennas*, *broadband antennas*, and *aperture antennas*. Balanis [26] also gives a good description of the common antenna types.

Wire Antennas are the most common type of antennas which come in various shapes: straight wire dipoles, loop antennas and helix antennas. *Aperture Antennas* consist of a kind of opening through which the electromagnetic waves are transmitted and received. Slot antennas, Waveguides, Horn antennas, Reflector antennas, and Lens antennas fall under this category of antennas. Aperture antennas are mainly used in aircraft and spacecraft applications. *Array Antennas* are used in applications where a single element does not provide sufficient radiation. They are formed by the arrangement of a number of antenna elements in a one or two-dimensional configuration. The configuration can be designed in such a manner as to achieve maximum radiation in the desired direction.

Microstrip Antennas, which are among the most useful antennas at microwave frequencies, are the antennas of utmost interest to this thesis. They are made up of a metal patch and a ground

plane separated by a dielectric substrate. The patch can take various shapes with the rectangular and circular patches being the most common due to ease of fabrication and good radiation performance. Some of the major advantages of microstrip antennas are that they are low-profile, easy to fabricate, may be used on planar and non-planar surfaces, and are mechanically robust. These are some of the reasons why the novel tag antenna designed in this thesis uses microstrip implementation. Microstrip antennas are described in more detail later in this chapter.

2.3 Performance Parameters of Antennas

The performance of an antenna is gauged through a number of parameters. It is through these parameters that an antenna can be selected for any application. Hence it is important to know the definition of these parameters which is available in [27]. The performance of the antennas designed in this thesis will also be analyzed based on some of these parameters which are explained below.

2.3.1 Radiation Pattern

The antenna radiation pattern is one of the most fundamental attributes of an antenna. Many of the parameters which determine antenna performance are derived from the radiation pattern. The radiation pattern is defined as "The spatial distribution of a quantity that characterizes the electromagnetic field generated by an antenna" [27]. It is commonly determined in the far-field region and its representation is in terms of the coordinates. The spherical coordinates system (r, θ, φ) is preferred over the Cartesian coordinate system (x, y, z) for the representation of the radiation pattern as it is simpler to express the electric field intensity over a spherical surface.

Radiation Pattern Lobes

The radiation pattern is made up of a number of parts which are known as *lobes*.

Figure 2-1 shows a typical 3-dimensional radiation pattern with the different types of lobes which are: *major*, *minor*, *side*, and *back* lobes.

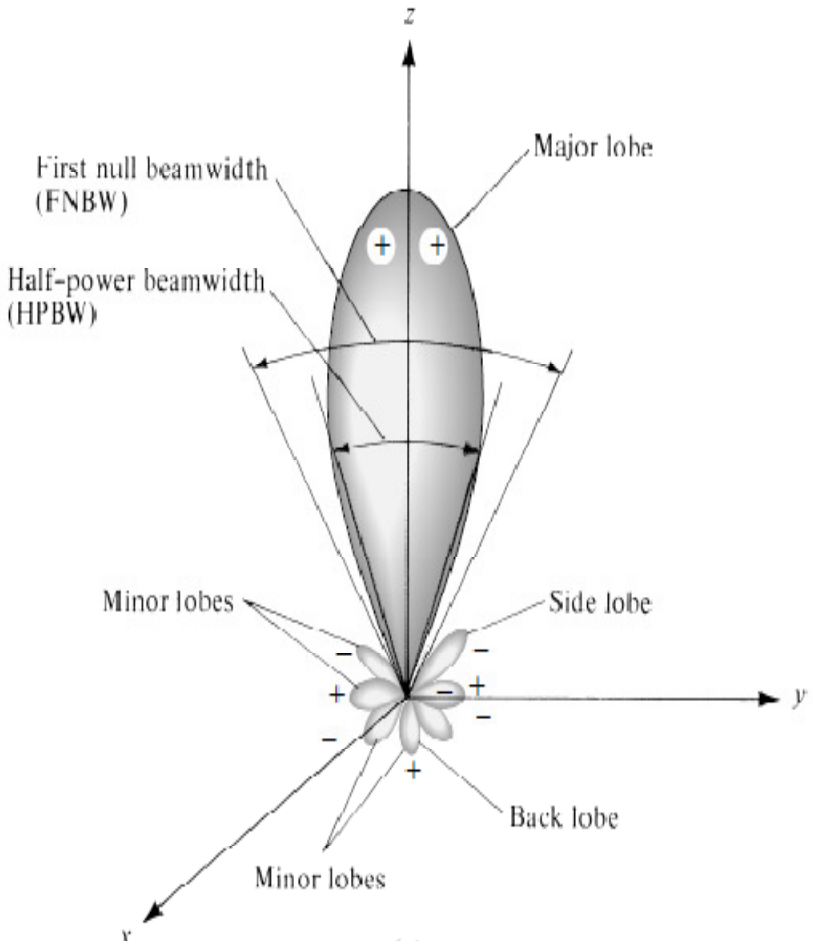

Figure 2-1 Radiation Lobes and Antenna Beamwidth [26]

The major lobe refers to the radiation lobe which has maximum radiation in the desired direction whereas a minor lobe is one which radiates in a direction other than the desired direction. A side lobe is any lobe which is not in the intended direction of radiation and a back lobe is one which is usually behind the plane of the antenna and radiating in the direction opposing the major lobe. A desirable antenna pattern would minimize the number of side and back lobes.

Radiation Field Regions

The space that surrounds the antenna is divided into 3 regions based on the distance from the antenna – *reactive near-field*, *radiating near-field* (Fresnel) and *far-field* (Fraunhofer) regions. The three regions are shown in Figure 2-2.

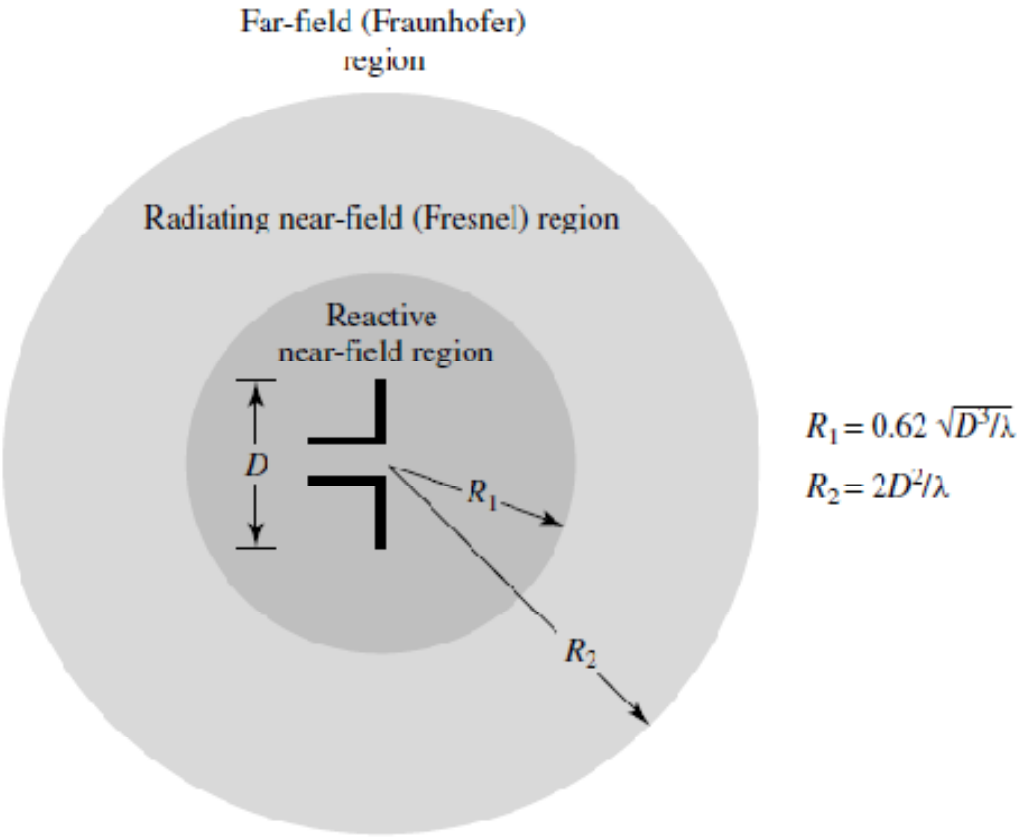

Figure 2-2 Antenna radiation regions [26]

Reactive near-field region, as the name suggests, is the region in the immediate proximity of the antenna where the dominating field is the reactive field. Radiating near-field (Fresnel) region is the region just beyond the reactive near-field region where the dominating field is the radiating field and the distance from the antenna determines the angular distribution of the field. Far-field

(Fraunhofer) region is the region beyond the Fresnel region where the radiation field dominates and the angular field distribution is independent of the distance from the antenna.

If λ is the wavelength, D is the largest antenna dimension, and R is the distance from the antenna, then the boundaries for the three regions is given as:

$$R \leq 0.62\sqrt{\frac{D^2}{\lambda}} \rightarrow \text{Reactive near-field region}$$

$$R \geq 0.62\sqrt{\frac{D^2}{\lambda}} \; and \; R < \frac{2D^2}{\lambda} \rightarrow \text{Fresnel region}$$

$$R \geq \frac{2D^2}{\lambda} \rightarrow \text{Fraunhofer region}$$

2.3.2 Antenna Directivity

The directivity of an antenna indicates the performance of an antenna in a particular direction. The IEEE Definitions of Antenna Terms [27] defines the directivity of an antenna as "the ratio of the radiation intensity in a given direction from the antenna to the radiation intensity averaged over all directions." The average radiation intensity is given as the total radiated power divided by 4π.

If U is the radiation intensity, U_0 is the average radiation intensity and P_{rad} is the total radiated power, then the directivity D is given as:

$$D = \frac{U}{U_0} = \frac{4\pi U}{P_{rad}}$$

2.3.3 Antenna Gain

A parameter that is closely associated with the antenna directivity is the antenna gain. It is a useful parameter for analyzing the performance of an antenna. The absolute gain of an antenna is defined by [27] as "the ratio of the intensity, in a given direction, to the radiation intensity that would be obtained if the power accepted by the antenna were radiated isotropically." The radiation intensity for the isotropically radiated input power is given as the input power divided by 4π.

If U is the radiation intensity, U_{in} is the radiation intensity for isotropically radiated input power and P_{in} is the input power, then the gain G is given as:

$$G = \frac{U}{U_{in}} = \frac{4\pi U}{P_{in}}$$

2.3.4 Antenna Efficiency

The antenna radiation efficiency (η_e) is given as the ratio of the total power radiated by the antenna (P_{rad}) to the total power accepted by the antenna (P_{in}).

$$\eta_{e=\frac{P_{rad}}{P_{in}}}$$

The antenna gain G and the antenna directivity D can be related as:

$$G = \eta_e D$$

The antenna efficiency η_e takes into account the dielectric and conduction losses as well as losses due to mismatch at the antenna terminals.

2.3.5 Input Impedance

The input impedance of an antenna is the impedance that the antenna presents at its input terminals. It can also be expressed as the ratio of the electric and magnetic field components at a point.

In mathematical form the impedance Z_A (ohms) is given as:

$$Z_A = R_A + jX_A$$

where R_A is the antenna resistance (ohms) and X_A is the reactance of the antenna (ohms).

The resistive component R_A (ohms) is expressed as:

$$R_A = R_r + R_L$$

where R_r is the radiation resistance and R_L is the loss resistance.

2.3.6 Antenna Bandwidth

The bandwidth of an antenna is the frequency band over which the performance of an antenna conforms to a specific standard with respect to a certain characteristic [26]. The center frequency within the bandwidth is the resonant frequency of the antenna. The bandwidth for broadband antennas is the ratio of the uppermost frequency of acceptable performance to the lowermost frequency of acceptable performance. The percentage of frequency difference over the center frequency is the bandwidth specification for narrowband antennas.

2.3.7 Return Loss and VSWR

The value of the return loss indicates the effectiveness of the impedance match between the transmission line and the antenna. It is expressed as a ratio of the power fed into the antenna and

the power reflected back to the source. The higher the value of the return loss, the better is the match between the line and the antenna.

$$RL\ (dB) = 10\log_{10}\frac{P_{in}}{P_{ref}}$$

where RL is the return loss expressed in dB, P_{in} is the input power and P_{ref} is the reflected power.

The return loss can also be expressed in terms of the reflection coefficient ρ,

$$RL\ (dB) = \ 10\log_{10}\frac{1}{\rho^2} = \ -20\log_{10}\rho$$

where the reflection coefficient ρ is given as

$$\rho = \frac{P_{ref}}{P_{in}}$$

Another parameter which describes the impedance match between the transmission line and the antenna is the Voltage Standing Wave Ratio (VSWR). It is the ratio of the maximum voltage to the minimum voltage of a standing wave. When the value of the VSWR is 1 it implies that the impedance match is perfect and there is no loss of power. However a VSWR of 1 is not attainable in practice and the value is usually higher.

2.3.8 Antenna Polarization

The polarization of an antenna is the polarization of the electromagnetic wave it transmits, which is the locus of the electric field vector as a function of time. Depending on the shape traced out by the electric field vector, polarization can be classified into three types: linear polarization, circular polarization and elliptical polarization.

Linear Polarization

When the electric field vector traces a straight line the wave is said to be linearly polarized. An antenna is said to be linearly polarized if it radiates a linearly polarized wave.

Circular Polarization

When the electric field vector traces out a circle, the wave is said to be circularly polarized. If the circle is traced in a clockwise rotation then it is called *right-hand circular polarization* and when it is traced in a counterclockwise rotation it is termed as *left-hand circular polarization*.

Elliptical Polarization

When the figure traced out by the electric field vector is an ellipse, the wave is said to be elliptically polarized. It is to be noted that linear and circular polarizations are special cases of elliptical polarization.

A parameter which can be used to determine the type of polarization is the *axial ratio*. It is a ratio of the orthogonal components of the electric field. The axial ratio is 1 for circular polarization as the field is made up of two orthogonal components of equal magnitude. It is greater than 1 for elliptical polarization while for linear polarization the axial ratio is infinite because the orthogonal component of the field is zero.

2.4 Microstrip Antennas

As mentioned earlier the antenna of utmost interest to this thesis is the microstrip antenna. The earliest work done on microstrip antennas was by Deschamps [28] in 1953 and a patent [29] applied in 1955. However, the first microstrip was built only in the year 1972 by Robert Munson [30][31], after which microstrip antennas became a popular topic of research. Microstrip

antennas can be designed for a wide range of frequencies, and working models have so far been developed for frequencies from about 400 MHz to 38 GHz.

2.4.1 Advantages and Disadvantages

There are several advantages and disadvantages of using microstrip antennas over conventional antennas.

2.4.1.1 Advantages

Some of the advantages of microstrip antennas are:

- Low Profile – they have a small form factor which is of utmost importance to modern applications where space is a constraint.
- Highly conformal – they can be made conformable to both planar and non-planar surfaces.
- Ease of manufacturing – they are simple to fabricate using modern printed circuit technology.
- Highly robust – they can be placed on rigid surfaces and are quite rugged.
- Ease of integration – they are compatible with MMIC designs and can be integrated easily with the circuit elements.
- Highly versatile – they can be designed for multi-frequency operations or for dual-polarization operations.

2.4.1.2 Disadvantages

Some of the drawbacks of using microstrip antennas are:

- Narrow bandwidth – they have a very narrow bandwidth in their basic form which is suitable only for certain applications. However there have been various methods proven to widen the bandwidth [32][33][34][35].
- Low power and efficiency – they cannot handle a large amount of RF power due to the minimal separation between the patch and the ground plane and are not highly efficient.
- High Q factor – they have a high Q factor sometimes in excess of 100.

2.4.2 Construction

Microstrip antennas consist of a very thin strip of metal placed a small fraction of a wavelength above a ground plane. A dielectric substrate separates the strip and the ground plane. The metal strip is commonly referred to as a patch. The geometry of a microstrip antenna is shown in Figure 2-3.

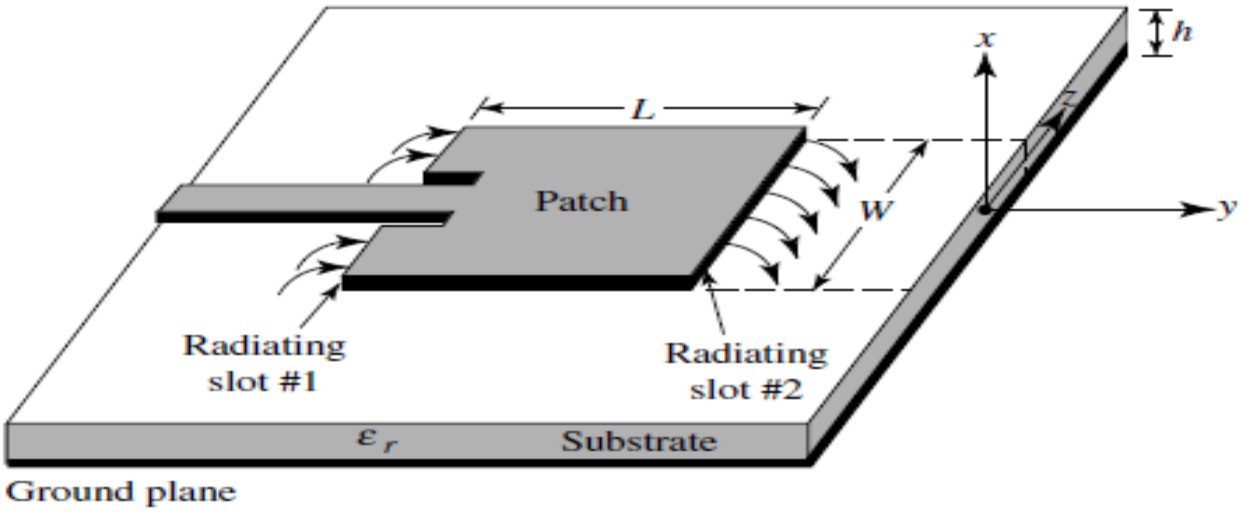

Figure 2-3 Microstrip antenna construction [26]

The conducting strip can be of any shape with the most common ones being a simple rectangular or circular patch. It could also be a resonant dipole, or an array of patches or dipoles along with their feed network [36].

2.4.3 Materials Used

The radiating top surface is normally made of thin copper. There are plenty of choices available for the dielectric substrate having dielectric constants ranging from as low as 1.17 to as high as 25 and loss tangents varying from 0.0001 to 0.004 [37][38]. A detailed overview of the various substrate materials available and their properties is provided in [36].

The considerations while selecting a dielectric substrate involves a trade-off between the cost, power loss, and performance. When a material with a high dielectric constant is used the size of the patch decreases significantly and the fabrication cost reduces, however the power loss increases and the performance is hence degraded. This was evidenced in this thesis when Rogers Duroid 5880 (ε_r= 2.2) and FR4 (ε_r = 4.4) were used to design the same antenna.

2.4.4 Feeding Techniques

There are four popular techniques for feeding microstrip antennas. A brief description of each of these methods is provided below.

2.4.4.1 Coaxial Probe Feed

This is the most common technique used to feed microstrip antennas. A coaxial probe is used to feed the antenna. The inner conductor of the coaxial cable is connected to the patch while the outer conductor is connected to the ground plane. The characteristic impedance of the coaxial probe is generally 50 ohms and hence the feed point on the patch should be at a point where the input impedance is 50 ohms, in order to achieve a good impedance match. Though the coaxial

probe is easy to fabricate and match, it has a narrow bandwidth and modeling becomes pretty complex as the thickness of the substrate increases.

2.4.4.2 Microstrip Line Feed

A microstrip transmission line is connected directly to the microstrip patch. In order to match the impedance at the edge of the patch, quarter-wavelength transformers are used. A simpler method to match the impedance is to extend the microstrip feed line into the patch. The microstrip line is easy to fabricate and the impedance can be easily matched by controlling the inset position. The drawback of this method is that as the thickness of the substrate increases the spurious radiations increase which limits the bandwidth of operation.

2.4.4.3 Proximity-Coupled Microstrip-Line Feed

This method uses an open-ended microstrip line to feed the patch antenna through proximity coupling. The open-ended line could be placed underneath the patch at the position where the impedance matches or it could also be placed in parallel close to the edge of the patch in which case the excitation is achieved through fringe-field coupling. The advantage of this method is that no soldering is required which increases the reliability.

2.4.4.4 Aperture-Coupled Feed

An open-ended microstrip line is placed on another substrate below the ground plane. There is a slot in the ground plane through which the patch on top of the ground plane is excited by the open-ended microstrip line situated below the ground plane. This method also avoids any soldered connection and also reduces the amount of spurious radiation. It also achieves a higher bandwidth when a thick substrate is used, which increases further when a resonant slot is used.

However this method is the most complex to model and the back radiation from the slot is a major drawback.

The book by Lee and Luk [39] provides a summary of advantages and disadvantages of using the four feeding techniques.

2.4.5 Analysis Techniques

Many techniques are employed for the analysis of microstrip antennas. The three methods that are generally used are: transmission-line model, cavity model and full-wave model.

Transmission-line Model

The easiest technique for modeling microstrip antennas is the transmission-line model which uses transmission-line theory and models the patch as two parallel radiating slots [31]. The main advantage of this technique is that it is a very simple method which provides good physical insight. However the drawback of this method is that it is not highly accurate and it is difficult to model mutual coupling [40].

Cavity Model

A more complex technique for modeling microstrip antennas is the cavity model. It is more accurate than the transmission-line model and also provides a good physical insight. However it is much more complex than the transmission-line model and coupling is difficult to model although there have been models that have successfully modeled coupling [41][42][43].

Full-wave Model

The most complex modeling technique for microstrip antennas is the full-wave model. The advantages of this technique, when used correctly, is that it is very accurate, very versatile, and can treat single elements, finite and infinite arrays, stacked elements, arbitrarily shaped elements, and also model mutual coupling [26]. The drawbacks of this method are that it is a very complex model and it does not provide good physical insight.

2.5 The Rectangular Patch Antenna

The most commonly used microstrip antenna is the rectangular patch antenna. In this thesis the rectangular patch antenna is used as a reference antenna. The theory behind the working of a patch antenna, its fundamental characteristics, and a transmission-line model for the patch is summarized in this section.

2.5.1 Geometry

The rectangular patch antenna is characterized by its length (L), width (W), substrate thickness (h) and relative permittivity (ε_r). The geometry of the rectangular patch is shown in Figure 2-4.

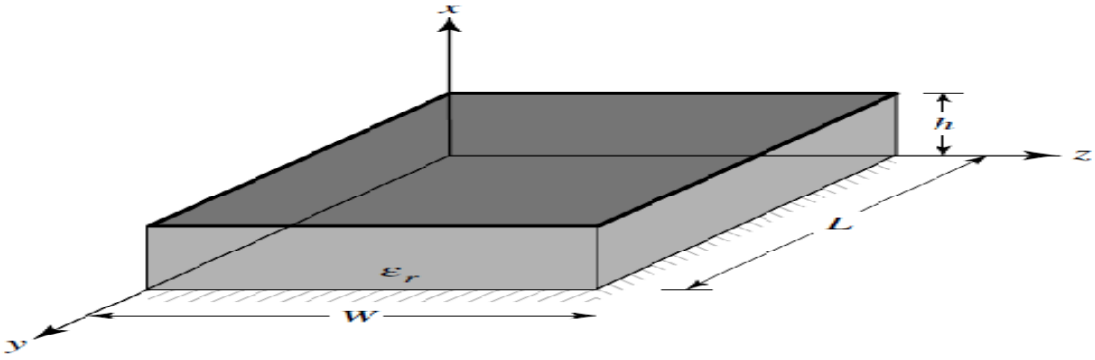

Figure 2-4 Rectangular patch antenna geometry [26]

Effective Length

The fringing edge effects cause the electrical length of the patch to appear longer than its physical length. The increase in length on each side (ΔL) is a function of the *W/h* ratio and the effective dielectric constant ε_{reff}. Hammerstad [45] gives an expression for the normalized length extension which is generally followed:

$$\frac{\Delta L}{h} = 0.412 \frac{\left(\varepsilon_{reff} + 0.3\right)\left(\frac{W}{h} + 0.264\right)}{\left(\varepsilon_{reff} - 0.3\right)\left(\frac{W}{h} + 0.8\right)}$$

The increase in the length of the patch is $2\,\Delta L$ and hence the effective length of the patch is:

$$L_{eff} = L + 2\Delta L$$

Resonant Frequency

The resonant frequency of the patch for the dominant TM_{010} mode including the fringing effects is a function of its length and is given by:

$$(f_{rc})_{010} = \frac{1}{2L_{eff}\sqrt{\varepsilon_{reff}}\sqrt{\mu_0\varepsilon_0}} = \frac{C}{2(L + \Delta L)\sqrt{\varepsilon_{reff}}}$$

where *C* is the speed of light in free space

2.5.2 Design Procedure

The steps for the design of a microstrip patch antenna can be outlined as follows:

- The initial step for the design of a rectangular patch antenna is the specification of the resonant frequency (f_r), the dielectric constant of the substrate (ε_r), and the height of the dielectric substrate (h).

- The width (W) of the patch, the effective dielectric constant (ε_r), and the extension of length (ΔL) are calculated using the equations described previously.
- Using the value of ΔL the actual length of the patch can be determined as:

$$L = \frac{1}{2f_r\sqrt{\varepsilon_{reff}}\sqrt{\mu_0\varepsilon_0}} - 2\Delta L$$

- The transmission-line model assumes the size of the ground plane to be infinite; hence a practical approximation of the size of the ground plane needs to be identified. It has been shown in [46] that a ground plane with dimensions that are greater than the patch dimensions by approximately 6 times the substrate height (h); provides results that are almost similar as those obtained with an infinite ground plane.

Chapter 3

Left-Handed and Composite Right/Left Handed Materials

3.1 Overview of Metamaterials

3.1.1 Introduction

The fundamental properties of a material which determine the propagation of electromagnetic waves through it are the permittivity ε and the permeability μ. For most naturally occurring materials the values of ε and μ are positive. However, materials with negative permittivity ε or negative permeability μ have been known to exist for a very long time. The Drude-Lorentz models actually predicts regions of negative ε or μ above each resonance if the losses are small enough [47]. There are many examples of materials which have negative ε such as low-loss plasmas, and semiconductors and metals at optical and infrared frequencies. However materials with negative μ are not very common as most solid-state materials have weak magnetic interactions [48]. Ferrimagnetic materials have strong magnetic interactions which produce regions with negative permeability. The non-reciprocity of these materials makes them very useful in Microwave engineering. The materials mentioned thus far possess either negative permittivity ε or negative permeability μ but not both simultaneously. The materials which possess both negative permittivity and negative permeability are of particular interest and are known as metamaterials.

Metamaterials are defined as artificial effective homogeneous electromagnetic structures with unusual properties and not readily available in nature [17]. A structure is said to be homogeneous when its average cell size is much smaller than the guided wavelength. *Left-Handed* (LH)

materials are the most popular form of metamaterials and are characterized by antiparallel phase and group velocities or by a negative index of refraction. Composite right/left handed materials are a generalization of LH metamaterials and are the basis of the research done in this thesis.

3.1.2 Evolution of the Theory of Left-Handed Materials

The idea of Left-Handed materials was first speculated in 1967 by Viktor Veselago [15]. The term Left-Handed was coined by Veselago because the electric field vector, magnetic field vector, and the wave vector formed a left-handed triplet as opposed to a right-handed triplet formed by substances with positive ε and μ. The major physical impact of left-handedness is backward-wave propagation which implies that the energy and the wavefronts travel in opposing directions. Some of the other names for left-handed materials are negative-refractive materials [49], backward materials [50], and double-negative materials [51].

Although the theory of left-handedness was proposed in 1967, it was only after three decades that it was proven experimentally. This was done by a group at the University of California, San Diego who proposed a LH metamaterial structure based on the work done by Pendry at the Imperial College at London [16]. Pendry created two structures, one with positive ε and negative μ and the other with negative ε and positive μ [52][53]. The two structures are the split-ring resonator structure (positive ε/negative μ) and the thin-wire structure (negative ε/positive μ).

The two structures created by Pendry were combined by the group at UCSD [16] to form a composite structure which was officially the first LH metamaterial to have been experimentally demonstrated. This structure provides a frequency range in which both the permeability and the permittivity have negative values. This was a mono-dimensional LH structure which was improved to create a bi-dimensional LH structure [54]. This structure is shown in Figure 3-1.

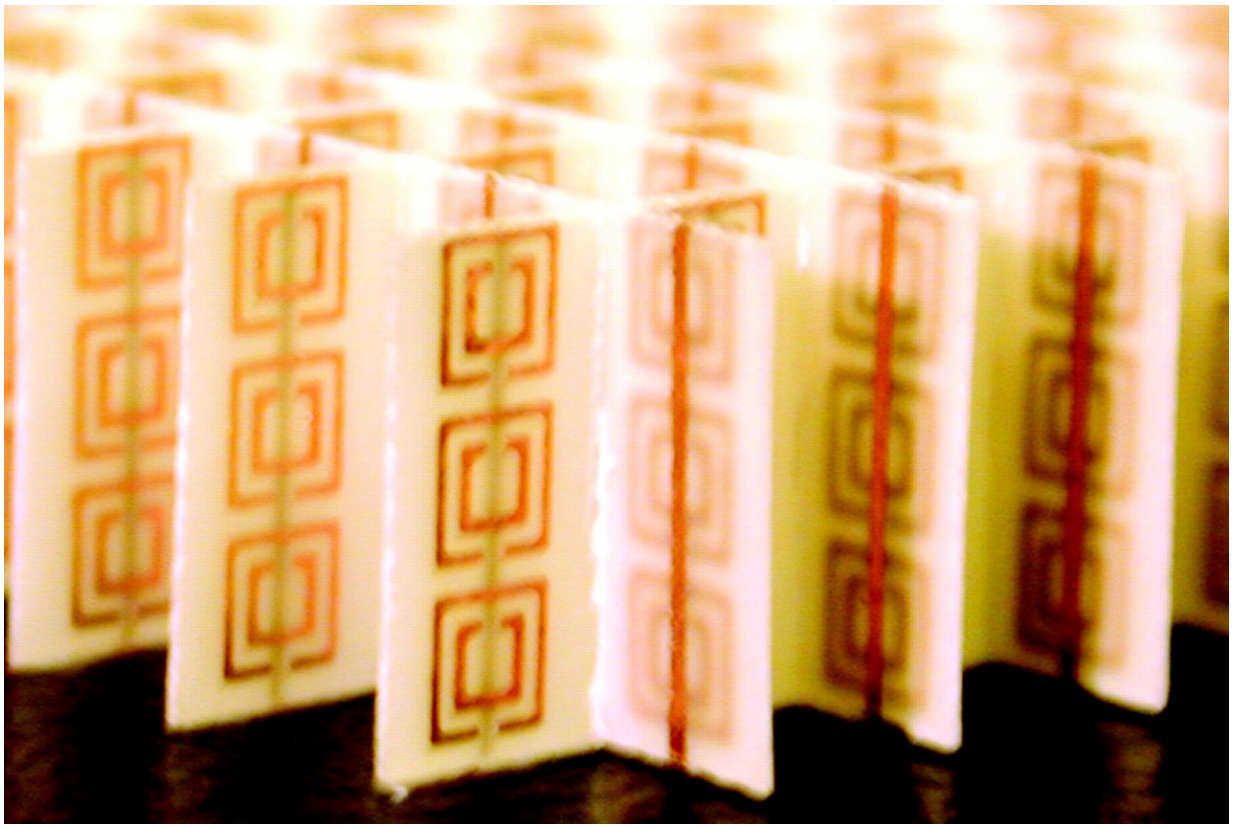

Figure 3-1 First experimental LH structure [54]

After the first experimental demonstration of LH metamaterials a number of publications emerged ratifying the theory of left-handed materials. Various numerical approaches have also been used to verify the concept of LH metamaterials [51][55][56][57][58][59]. Some of the works confirming the theory are [50][60][61][62][63][64] and other experimental confirmation can be found in [54][64][65][66].

3.2 Special Properties of Left-Handed Metamaterials

There has been tremendous interest in LH metamaterials ever since they were experimentally verified. The main reason for this interest is the extraordinary properties that they exhibit. Some of the physical phenomena which occur in natural (right-handed) materials are seen to be totally

reversed in LH materials. This makes the LH materials very useful for a lot of existing and novel applications. Some of the special properties of LH materials are explained in this section.

3.2.1 Backward Wave Propagation

Backward wave propagation is essentially the origin of the term 'left-handed' materials by Veselago [15]. It can be better explained by initially considering the wave form of Maxwell's equations:

$$\left(\nabla^2 - \frac{\eta^2}{c^2}\frac{\partial^2}{\partial t^2}\right)\psi = 0$$

where η is the refractive index and c is the velocity of light in vacuum, which are related as:

$$\frac{\eta^2}{c^2} = \varepsilon\mu$$

Hence when the square of the refractive index is considered there is no effect due to the simultaneously negative values of ε and μ. The intuition from this is that the solutions to the Maxwell's equation in wave form do not change even with simultaneously negative values of ε and μ.

However considering Maxwell's equations in differential form:

$$\nabla\ X\ \boldsymbol{E} = -j\omega\mu\boldsymbol{H} \text{ and } \nabla\ X\ \boldsymbol{H} = j\omega\varepsilon\boldsymbol{E}$$

Now it is intuitive that for simultaneously negative values of ε and μ the solutions are quite different. The electric and magnetic field vectors for a planar wave are given as:

$$\boldsymbol{E} = \boldsymbol{E}_0 e^{(-j\boldsymbol{k}.\boldsymbol{r}+j\omega t)}$$

$$\boldsymbol{H} = \boldsymbol{H}_0 e^{(-j\boldsymbol{k}.\boldsymbol{r}+j\omega t)}$$

which can be reduced to:

$$\boldsymbol{k}\, X\, \boldsymbol{E} = \omega\mu\boldsymbol{H}$$

$$\boldsymbol{k}\, X\, \boldsymbol{H} = -\omega\varepsilon\boldsymbol{E}$$

From these two equations it is evident that for positive values of ε and μ, the electric field, magnetic field, and wave vectors form a right-handed triplet.

For negative values of ε and μ,

$$\boldsymbol{k}\, X\, \boldsymbol{E} = -\omega|\mu|\boldsymbol{H}$$

$$\boldsymbol{k}\, X\, \boldsymbol{H} = \omega|\varepsilon|\boldsymbol{E}$$

which indicates that the E, H, and k vectors now form a left-handed triplet.

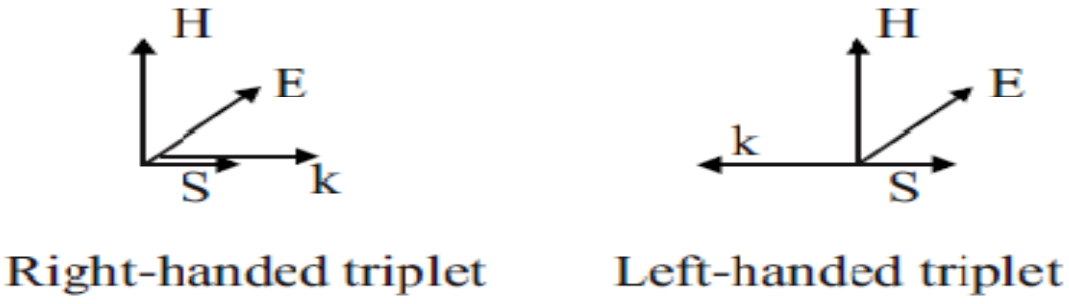

Figure 3-2 System of vectors E, H, S, and k in conventional and Left-Handed media

The impact of the above result, as can be seen in Figure 3-2, is that the propagation of the wave is now in a direction opposite to that in a normal (right-handed) material. It is also important to

note that the direction of the Poynting vector **S** does not change. This phenomenon is referred to as *Backward-wave* propagation.

3.2.2 Negative Refractive Index

One of the most interesting properties of LH materials is the reversal of the fundamental Snell's law of refraction. According to Snell's law:

Where η_1 is the refractive index of the incident medium, η_2 is the refractive index of the refracted medium, θ_1 is the angle of incidence, and θ_2 is the angle of refraction.

When both the incident and the refracted media are ordinary materials, the angle of incidence and the angle of refraction have the same signs. However when the refracted medium is a LH material θ_1 and θ_2 have opposite signs. This follows directly from the concept of Backward-wave propagation in LH materials which was explained in the previous section. This phenomenon is shown in Figure 3-3 where $\theta_1 = \theta_2 = 8$ degrees for a conventional material and $\theta_2 = -8$ degrees for a left-handed metamaterial.

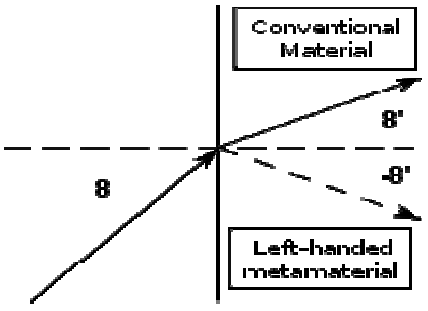

Figure 3-3 Refraction in conventional and LH materials

Hence it follows that when the refracted medium is a LH material,

$$\frac{\sin\theta_1}{\sin\theta_2} = \frac{\eta_2}{\eta_1} < 0$$

Since the refractive index of any ordinary material is positive, $\eta_1 > 0$. This implies than the refractive index of the LH metamaterial, $\eta_2 < 0$. The implication of this result is that when LH materials are used, convex lenses which are normally convergent become divergent and concave lenses which are normally divergent become convergent [15].

3.2.3 Reversal of Doppler Effect

A popular concept useful in many applications is the Doppler Effect which is the shift in the frequency of the wave observed from a source depending on the relative velocity of the observer and the source. For an ordinary medium this implies that when the observer is moving towards the source, the wave and the observer are moving in opposite directions and hence the frequency of the wave shifts upwards. The frequency shifts downwards when the observer moves away from the source.

However in a LH medium, backward wave propagation occurs and hence when the observer moves towards the source the wave propagates in the same direction and hence the frequency shifts downwards. The frequency shifts upwards when the observer moves towards the source. This is a reversal of the Doppler Effect described above. This has been proven both theoretically [15][17] and experimentally [67].

3.3 Transmission Line (TL) Theory for LH Metamaterials

The LH structures initially designed in [16] are lossy resonant structures and have very narrow bandwidth. This drawback precluded their use in many applications and other alternative approaches were proposed. One of the approaches, which provided a more useful structure, was

the Transmission Line (TL) approach [63][68][69][70][71]. A basic cell consisting of an inductor and a capacitor, which is the dual of a simple LC circuit, is an ideal LH TL and is proven to exhibit the properties of LH materials [17]. The LC equivalent circuit model for a homogeneous RH TL and a homogeneous LH TL are shown in Figure 3-4.

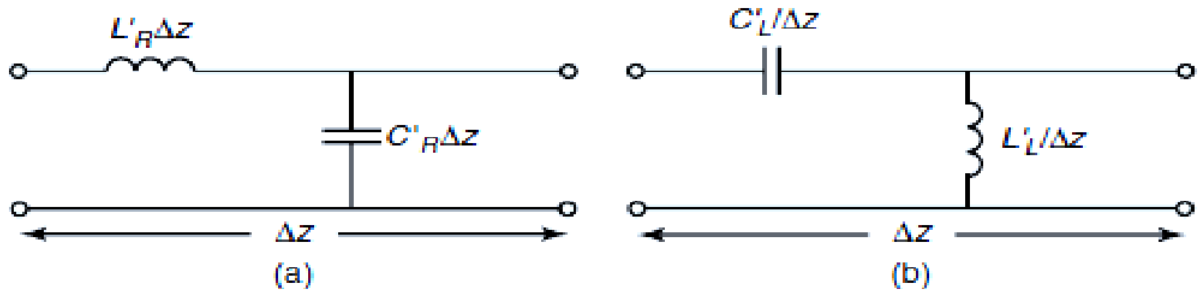

Figure 3-4 Equivalent circuit model (a) Homogeneous RH TL (b) Homogeneous LH TL[72]

The circuit model for the homogeneous RH TL consists of a series inductance L'_R per-unit length and shunt capacitance C'_R per-unit length. The circuit model for the homogeneous LH TL can been seen to be the dual of the RH TL case and consists of a series capacitance C'_L times-unit length and a shunt inductance L'_L times-unit length. From this result it was evident that a LH TL medium could be created with a cascade of such cells with the condition that the cell size is much smaller than the guided wavelength. Such a structure was proposed by [70] and was found to be nonresonant with low loss and a high bandwidth.

3.3.1 Advantages of TL Metamaterial Structures

The LH metamaterial structures realized through the transmission line theory have a number of advantages over the earlier structures. Some of the advantages are:

- The structures are nonresonant in nature. This implies that they have low loss and broad operating bandwidth.

- The resonant frequency of the structure is determined by the LC parameters which can be controlled easily.
- The structures can be designed in planar configurations.
- They are easily compatible with modern microwave integrated circuits.
- Since the transmission line theory has been thoroughly researched, the structures can be efficiently designed for microwave applications.

3.4 Composite Right/Left Handed (CRLH) Metamaterials

The ideal LH transmission line detailed in the previous section is hypothetical and cannot be realized in practice. This is due to the presence of a series inductance caused by current flow in the metal and a shunt capacitance caused by voltage gradients. This implied that a structure cannot be purely left-handed and led to the introduction of the term *Composite Right/Left Handed* (CRLH) for such materials [73][74].

3.4.1 CRLH Transmission Line (TL) Theory

The fundamental characteristics of CRLH metamaterials can be understood by analyzing the equivalent TL model [17]. For ease of analysis an ideal homogeneous loss-less TL is initially considered. Although an ideal homogeneous CRLH TL cannot be realized in practice, artificial structures which provide effective homogeneity can be constructed and hence the analysis of the ideal case does describe the fundamental properties of the CRLH metamaterials. The equivalent LC circuit model for a homogeneous loss-less CRLH TL is shown in Figure 3-5.

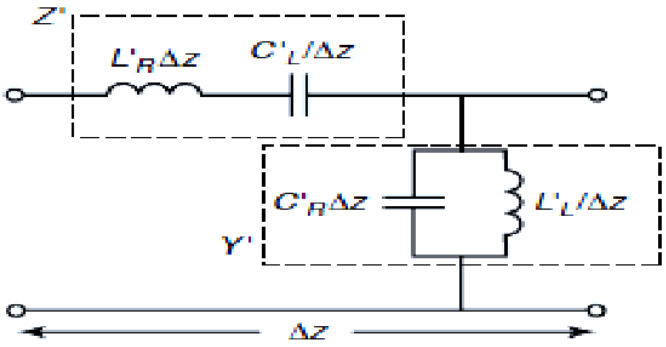

Figure 3-5 Equivalent circuit model for a homogeneous CRLH TL[72]

It can be seen from Figure 3-5 that the model for a homogeneous CRLH TL is a combination of the circuits described for RH and LH TLs. The series arm of the circuit consists of an inductance L'_R and a capacitance C'_L in series, while the shunt arm consists of a capacitance C'_R and an inductance L'_L in parallel. The impedance per-unit length (Z') and the admittance per-unit length (Y') are a function of frequency and are given as:

—

—

The equation for the propagation constant γ of a TL is:

—

where α denotes the attenuation and β denotes the dispersion.

The characteristic impedance of the TL is given as:

$$Z_C = R_C + jX_C = \frac{Z'}{\gamma} = \sqrt{\frac{Z'}{Y'}} = Z_C(\omega)$$

The dispersion relation for a homogeneous CRLH TL can be written as:

$$\beta(\omega) = s(\omega)\sqrt{\omega^2 L'_R C'_R + \frac{1}{\omega^2 L'_L C'_L} - \left(\frac{L'_R}{L'_L} + \frac{C'_R}{C'_L}\right)}$$

Where *s(ω)* is a sign function which is given as:

$$s(\omega) = \begin{cases} -1 \; if \; \omega < \min(\omega_{se}, \omega_{sh}) \\ +1 \; if \; \omega > \max(\omega_{se}, \omega_{sh}) \end{cases}$$

Here ω_{se} and ω_{sh} are the series and shunt resonance frequencies which are expressed as:

$$\omega_{se} = \frac{1}{\sqrt{L'_R C'_L}}$$

$$\omega_{sh} = \frac{1}{\sqrt{L'_L C'_R}}$$

When the sign function takes on a positive value the phase constant β is purely real and there exists a pass band since $\gamma = j\beta$. This is a typical characteristic of a RH TL. However when the sign function is negative the phase constant is purely imaginary and a stop band is present since $\gamma = \alpha$. This stop band characteristic is unique to the CRLH TL.

Figure 3-6 shows the dispersion diagrams for homogeneous RH, LH, and CRLH TLs. β is the phase constant and *c* is the speed of light in free space. Since the group velocity of a TL is $v_g = \partial\omega/\partial\beta$ and the phase velocity of a TL is $v_p = \omega/\beta$, they can be obtained from the dispersion diagram. It is evident that for a purely RH TL the phase and group velocities are

parallel (have the same sign) as , whereas for a purely LH TL which implies that the phase and group velocities are antiparallel (have opposite signs).

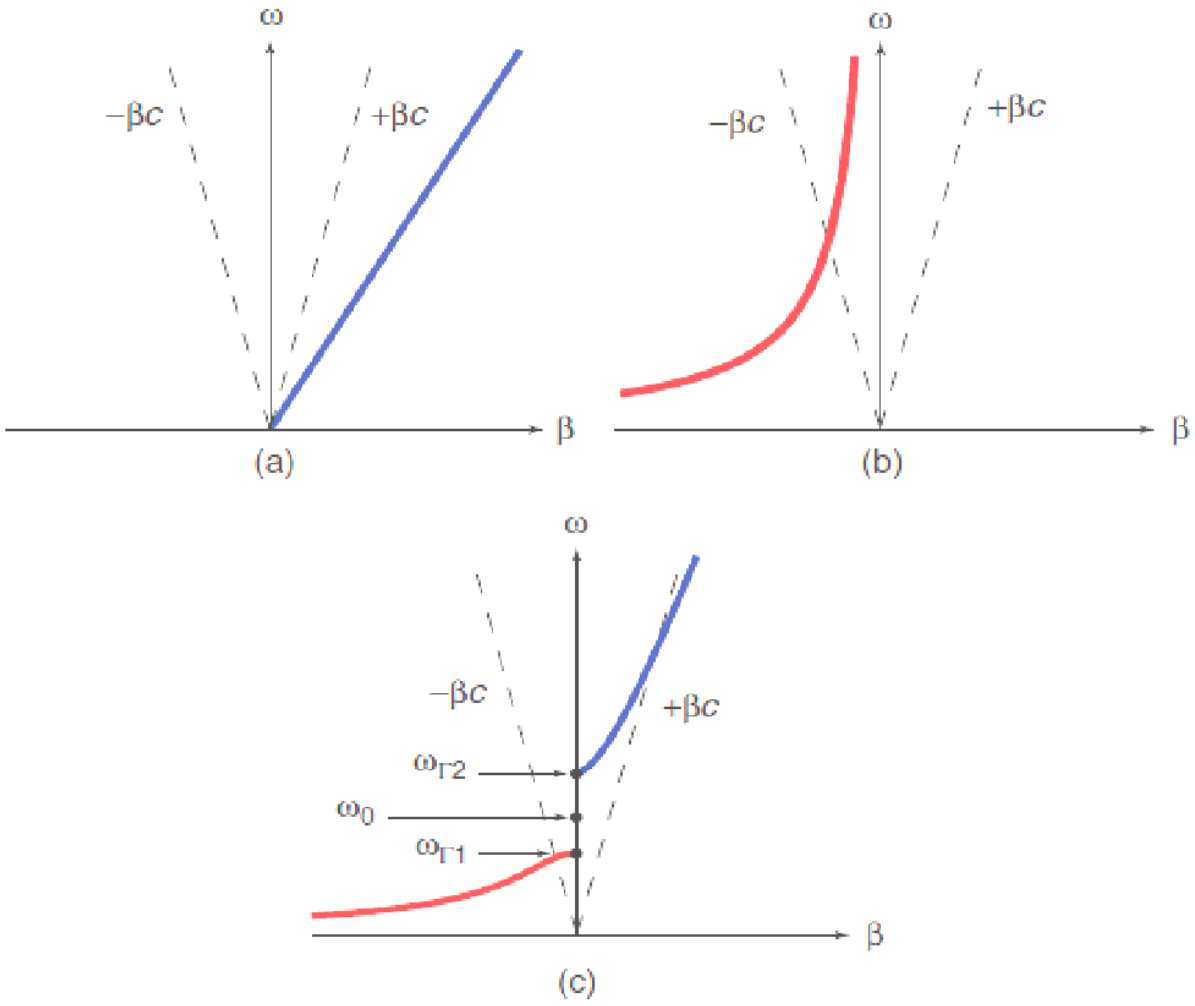

Figure 3-6 Dispersion diagrams (a) Homogeneous RH TL (b) Homogeneous LH TL (c) Homogeneous CRLH TL[72]

In the case of the CRLH TL it can be seen that there exists a band where the phase and group velocities are parallel (RH region) and a band where the phase and group velocities are antiparallel (LH region). There is also a band gap which occurs when γ is purely real. This is due to the difference in the shunt and series resonant frequencies (ω_{sh} and ω_{se}), and the CRLH TL is

then said to be *unbalanced* [17]. The CRLH TL is said to be balanced when the shunt and the series resonances are equal in which case the band gap disappears and there is smooth transition from the LH region to the RH region [72]. This is shown in Figure 3-7(b). The equivalent circuit model for a balanced CRLH TL is also shown in Figure 3-7(a).

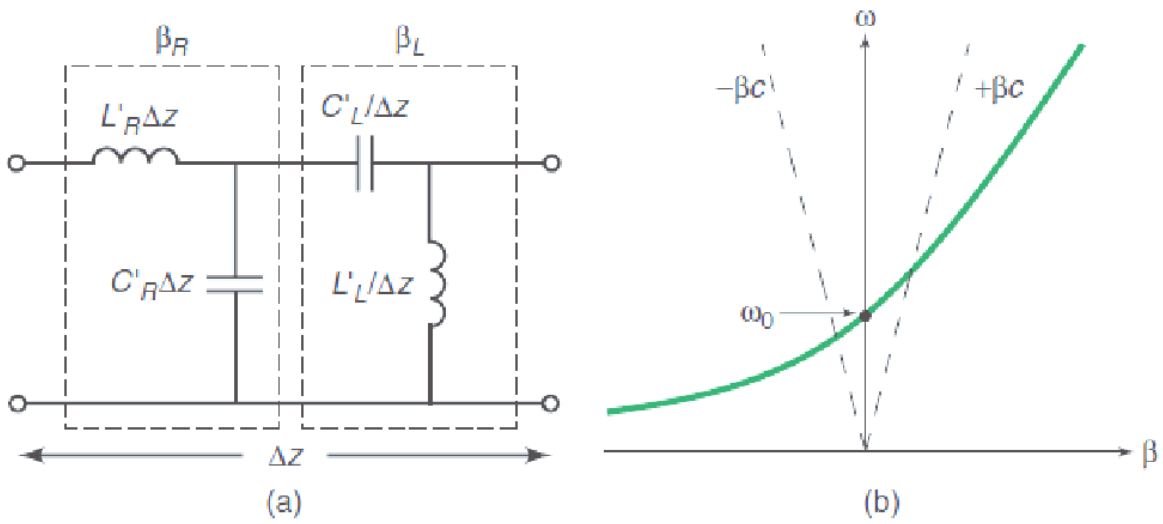

Figure 3-7 Balanced Homogeneous CRLH TL (a) Equivalent circuit (b) Dispersion diagram[17][72]

In the balanced CRLH TL the phase constant β can be split into two parts, one representing the RH phase constant (β_R) and the other representing the LH phase constant (β_L). This can be written as:

where

$$\beta_L = \frac{-1}{\omega\sqrt{L'_L C'_L}}$$

This indicates that at low frequencies the CRLH TL is essentially LH and less dispersive while at higher frequencies the CRLH TL is essentially RH and becomes more dispersive. This can be clearly seen in the dispersion diagram in Figure 3-7(b). The frequency at which the CRLH TL moves from the LH region to the RH region is termed as the *transition frequency* (ω_0), which is given as:

$$\omega_0 = \frac{1}{\sqrt[4]{L'_R C'_R L'_L C'_L}}$$

For the balanced CRLH TL, this reduces to:

$$\omega_0 = \frac{1}{\sqrt{L'C'}}$$

The transition frequency is also the frequency at which the maximum attenuation occurs [17]. Also, at the transition frequency the phase constant $\beta=0$ which implies that the guided wavelength is infinite. However, since the group velocity $v_g > 0$ wave propagation still occurs at this frequency.

The characteristic impedance of the unbalanced CRLH TL can now be written as:

$$Z_C = Z_L\sqrt{\frac{L'_R C'_L \omega^2 - 1}{L'_L C'_R \omega^2 - 1}}$$

For the balanced case this reduces to:

$$Z_C = Z_L = Z_R$$

where the impedance contribution of the LH part is $Z_L = \sqrt{\frac{L_L'}{C_L'}}$ and the impedance contribution of the RH part is $Z_R = \sqrt{\frac{L_R'}{C_R'}}$.

3.4.1.1 Relation of CRLH TL Parameters to the CRLH Metamaterial Parameters

The TL parameters that were derived in the previous sections can be related to the actual constitutive parameters of the CRLH metamaterial [17][72].

Propagation Constant

The propagation constant γ for a CRLH TL, as seen in the previous section, is given as:

$$\gamma = j\beta = \sqrt{Z'Y'}$$

In the case of a CRLH metamaterial, the propagation constant is expressed as:

$$\beta = \omega\sqrt{\mu\varepsilon}$$

Squaring and equating the two expressions, a relationship for the parameters can be written as:

$$-\omega^2\mu\varepsilon = Z'Y'$$

Characteristic Impedance

For the CRLH TL the characteristic impedance is given as:

$$Z_C = \sqrt{\frac{Z'}{Y'}}$$

The intrinsic impedance of the metamaterial is given by the equation:

$$\eta = \sqrt{\frac{\mu}{\varepsilon}}$$

These two expressions can be related as:

$$\frac{Z'}{Y'} = \frac{\mu}{\varepsilon}$$

From the two relations, the permittivity and permeability of the metamaterial can be written in terms of the impedance and admittance of the TL.

$$\mu = \frac{Z'}{j\omega} = L'_R - \frac{1}{\omega^2 C'_L}$$

$$\varepsilon = \frac{Y'}{j\omega} = C'_R - \frac{1}{\omega^2 L'_L}$$

3.4.1.2 Advantages of Balanced CRLH TL over Unbalanced CRLH TL

From the results derived in the previous sections, a number of advantages of Balanced CRLH TLs over their unbalanced counterparts can be identified. They can be summarized as:

- There is no coupling between the LH and RH parts of the balanced CRLH TL circuit. This makes it much simpler than the unbalanced model.
- There is no stop band in the balanced CRLH which results in a smooth transition between the LH and RH regions, whereas there is a band gap in the unbalanced case.
- From the expression derived for the characteristic impedance, it is evident that for the balanced CRLH TL the characteristic impedance is independent of the frequency. This implies that the balanced CRLH TL can be matched over a broad bandwidth. However this is not true in the case of the unbalanced CRLH TL where the characteristic

impedance is dependent on the frequency and hence can be matched only over a very narrow bandwidth.

- In the balanced CRLH TL there is wave propagation even at the transition frequency as the group velocity is not zero, whereas in the case of the unbalanced CRLH TL the group velocity is zero within the stop band.
- An extension of the previous point is that the phase shift at the transition frequency, $\varphi = -\beta l = 0$. This becomes positive when the frequency decreases (LH region), and becomes negative when the frequency increases beyond the transition frequency (RH region).

3.4.2 L-C Based CRLH TL Model

The ideal homogeneous CRLH TL described in the previous section is not practically realizable and is purely theoretical. However it is possible to realize an effectively homogeneous CRLH TL within a specific frequency band using an LC-based ladder network circuit structure [17].

The LC-based CRLH model is obtained by a cascade of LC unit cells shown in Figure 3-8(a). The resultant ladder network is shown in Figure 3-8(b). It is notable that unlike the basic LC model introduced in the ideal homogeneous case the unit cell in this case is not associated with a physical length (Δz) and is dimensionless. The size of the structure is represented in terms of its electrical length $\theta = |\Delta\varphi|$ (rad). It is proved in [17] that, if the length of the footprint of the unit cell $p = \Delta z \to 0$ this LC model becomes equivalent to the basic model in Figure 3-5. This condition is known as the homogeneity condition which ensures that the TL is seen to be effectively homogeneous. For the practical case the homogeneity condition translates to $p < \frac{\lambda_g}{4}$ where λ_g is the guided wavelength, and the electrical length $\theta < \frac{\pi}{2}$.

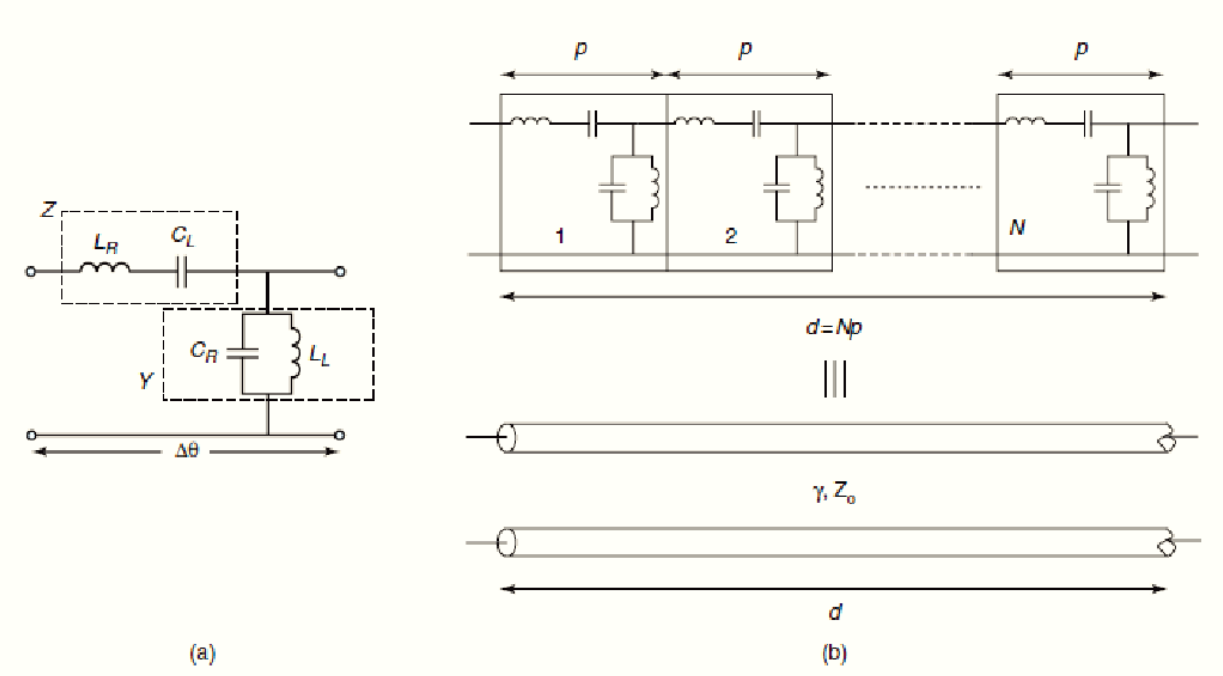

Figure 3-8 LC-Based CRLH Model (a) Unit cell (b) Periodic ladder network [72]

The impedance (Z) and the admittance (Y) of the unit cell are given as [17]:

As in the case of the ideal homogeneous TL, the series and shunt resonant frequencies are defined as:

The dispersion relation of the LC unit cell is found by applying the Bloch-Floquet theorem [17]:

$$\beta(\omega) = \frac{1}{p}\cos^{-1}\left(1 + \frac{ZY}{2}\right)$$

The Taylor's approximation $\cos\beta p \approx 1 - \frac{\beta p^2}{2}$ is applicable because the electrical length of the LC unit cell is very small. Also using the expressions for Z and Y given previously, the dispersion relation now becomes:

$$\beta(\omega) = \frac{s(\omega)}{p}\sqrt{\omega^2 L_R C_R + \frac{1}{\omega^2 L_L C_L} - \left(\frac{L_R}{L_L} + \frac{C_R}{C_L}\right)}$$

This expression shows that, at small electrical lengths this model is equivalent to the ideal homogeneous CRLH TL model. Although the LC-based CRLH TL model is seen to exhibit band pass filter properties there is no relation between the CRLH TL design and filter design [17].

3.4.3 Microstrip Implementation

The LC-based model discussed in the previous section needs to be physically implemented to design a CRLH TL structure. The two popular methods for physically implementing the LC network are through surface-mount technology (SMT) chip components or by using distributed components. A popular method of implementing distributed components is the microstrip implementation. This method of implementation is chosen because of it is easy to meet the design specifications such as the frequency of operation and phase responses.

The first distributed microstrip CRLH TL structure that was realized consisted of interdigital capacitors and stub inductors which were shorted to the ground by a via [17][64][75]. This structure is shown in Figure 3-9. The unit cell of this structure is equivalent to the unit cell of the

LC-based model seen in Figure 3-8(a). The C_L and L_L are contributed by the interdigital capacitors and the stub inductors while C_R and L_R are contributed by their parasitic reactances.

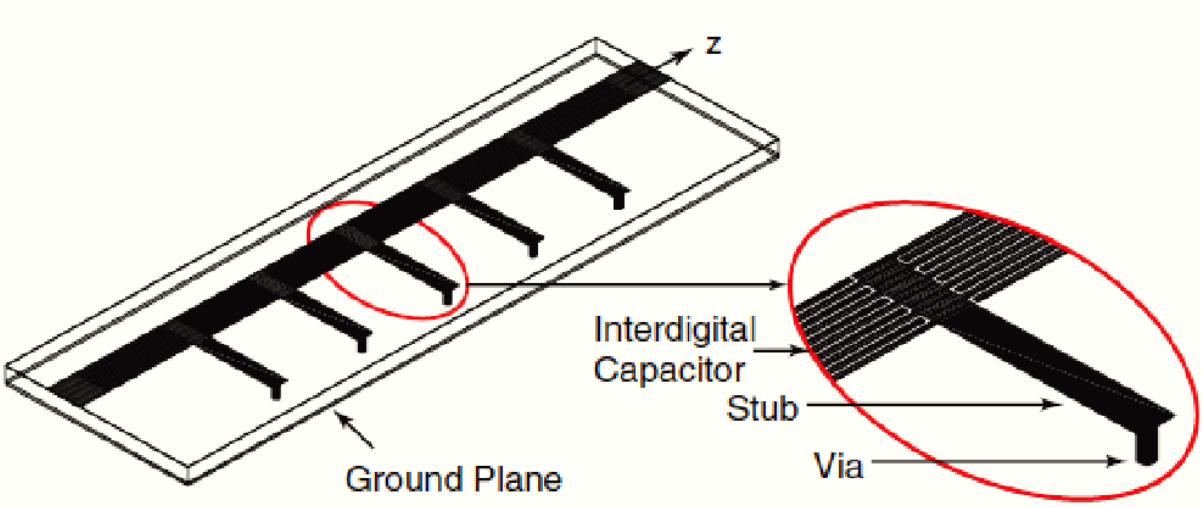

Figure 3-9 Microstrip CRLH with Interdigital capacitors and stub inductors [72]

A CRLH prototype based on this model was designed in [17] with 24 unit cells. The experimental and simulated results provided by this prototype showed a very good similarity with the LC network model over a wide bandwidth, thus ratifying the models developed for the characterization of the CRLH metamaterials. This prototype is shown in Figure 3-10.

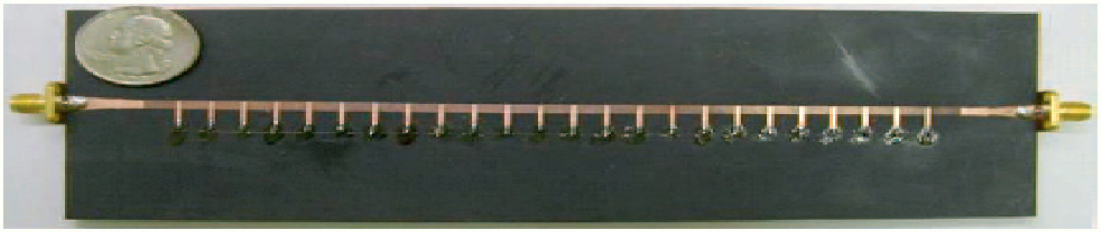

Figure 3-10 24-cell Microstrip CRLH TL prototype [72]

3.5 Radiation Applications of CRLH Metamaterials

The ability of the CRLH metamaterial structures to radiate is of tremendous interest and leads to a number of applications. Radiation occurs when the metamaterial structure is left open to free space and supports the leaky-wave (LW) mode. This property leads to the use of CRLH metamaterial structures as antennas or reflectors. There have been many applications designed using the LW mechanism, such as a Backfire-to-Endfire LW antenna, an electronically scanned LW antenna, and Reflecto-Directive structures [17]. However the primary application of interest to this thesis is the *Zeroth Order Resonating* (ZOR) antenna, which unlike the previous applications is based on a resonance mechanism rather than the LW mechanism.

3.5.1 Zeroth Order Resonating (ZOR) Antenna

The Zeroth Order Resonating antenna is based on the concept of the Zeroth Order Resonator (ZOR) which is explained in the next section. A LC network implementation and a Microstrip realization for the ZOR are then explained. This is the fundamental basis of the antenna designed in this thesis.

3.5.1.1 ZOR Principle

The CRLH TL, when open-ended or short-ended, produces standing waves as opposed to travelling waves. When this occurs the CRLH TL becomes a resonator. This characteristic is not

unique to CRLH TLs and occurs even in a RH TL. However the resonance characteristics of the CRLH TL are unique as even negative and zeroth-order resonances are allowed, which is not the case for a RH TL resonator.

For the conventional resonator the resonant frequencies are the frequencies where the physical length of the structure (l) is a multiple of $\lambda/2$ which equates to the electrical length (θ) being a multiple of π. Since the phase constant for a RH TL is always positive ($\beta>0$), the electrical length ($\theta= \beta l$) can only have a positive value. This implies that only positive resonances are allowed in a purely RH TL.

In the case of the CRLH TL it has been seen that the value of β at the transition frequency is 0, and is negative in the LH region. This implies that the electrical length may be zero ($\beta =0$, $\lambda g=$ *infinity*) and can take even negative values. Hence for an ideal CRLH TL resonator with physical length l, the condition for resonance to occur is:

$$\beta_n = \frac{n\pi}{l} \qquad (n = 0, \pm 1, \pm 2, \dots)$$

The resonant modes in the CRLH resonator are shown in **Figure 3-11**. The zeroth mode ($n=0$) is of particular interest because it corresponds to a flat field distribution and hence is independent of the physical length of the TL. This characteristic can theoretically be used to design very small resonators.

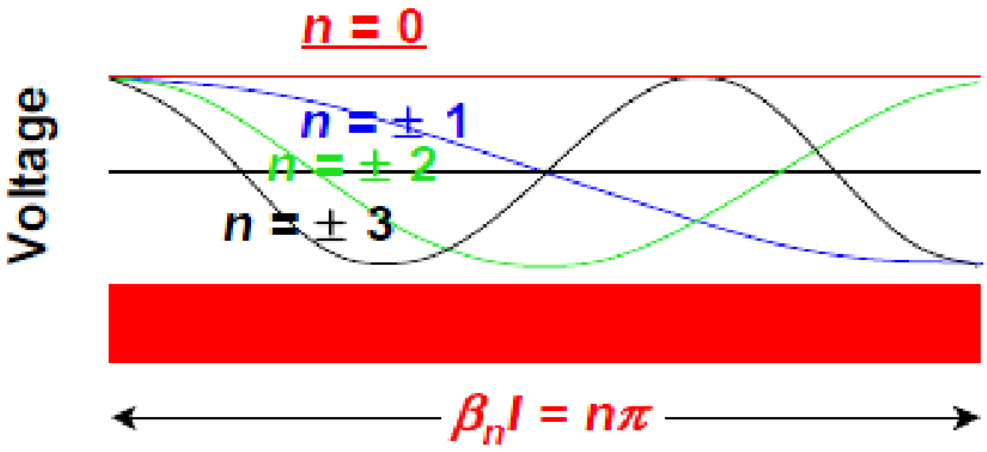

Figure 3-11 Modes of resonance in a CRLH TL resonator[74]

3.5.1.2 LC Implementation

The CRLH TL considered in the previous section is a theoretical case. The equivalent circuit of a practically realizable CRLH TL consisting of a cascade of unit cells is shown in Figure 3-12. A major difference between the ideal case and the LC network implementation is that the bandwidth is infinite for the ideal case while it is limited for the LC-network implementation.

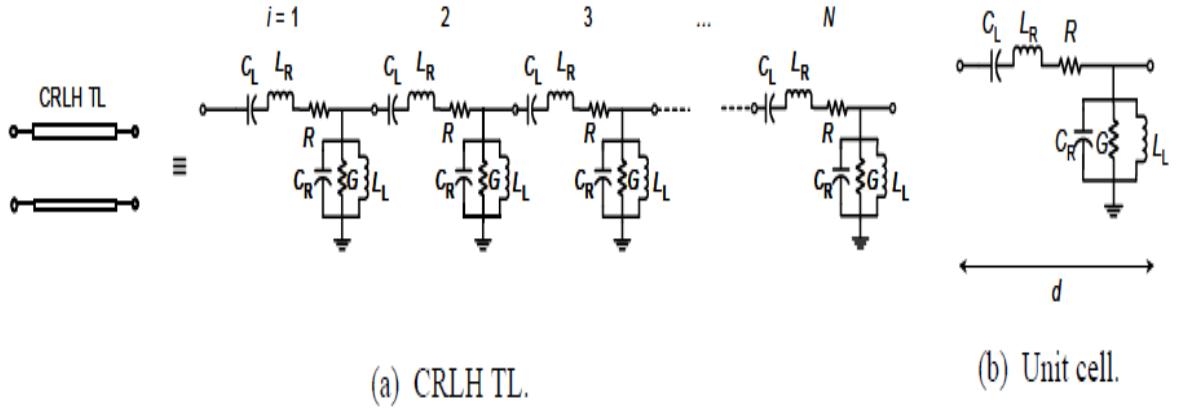

Figure 3-12 Equivalent circuit models[74]

The resonant frequencies of the CRLH TL in this case can be found by applying the Bloch-Floquet theorem to the unit cell of the structure [74].

$$\beta_n d = \frac{n\pi d}{l} = \frac{n\pi}{N} = \cos^{-1}\left\{1 - \frac{1}{2}\left[\frac{\omega_L^2}{\omega_n^2} + \frac{\omega_n^2}{\omega_R^2} - \left(\frac{\omega_L^2}{\omega_{se}^2} + \frac{\omega_L^2}{\omega_{sh}^2}\right)\right]\right\}$$

where $n = 0, \pm 1, \pm 2, \ldots, \pm N - 1$, d is the length of the unit cell, N is the number of unit cells, and the frequencies are defined as:

$$\omega_L = \frac{1}{\sqrt{L_L C_L}}, \omega_R = \frac{1}{\sqrt{L_R C_R}}$$

$$\omega_{se} = \frac{1}{\sqrt{L_R C_L}}, \omega_{sh} = \frac{1}{\sqrt{L_L C_R}}$$

The solutions for the resonant frequencies are shown in the dispersion diagram of the CRLH TL (assuming lossless case) in Figure 3-13. It can be seen from the diagram than the resonant frequencies are found at multiples of π/N along the β axis.

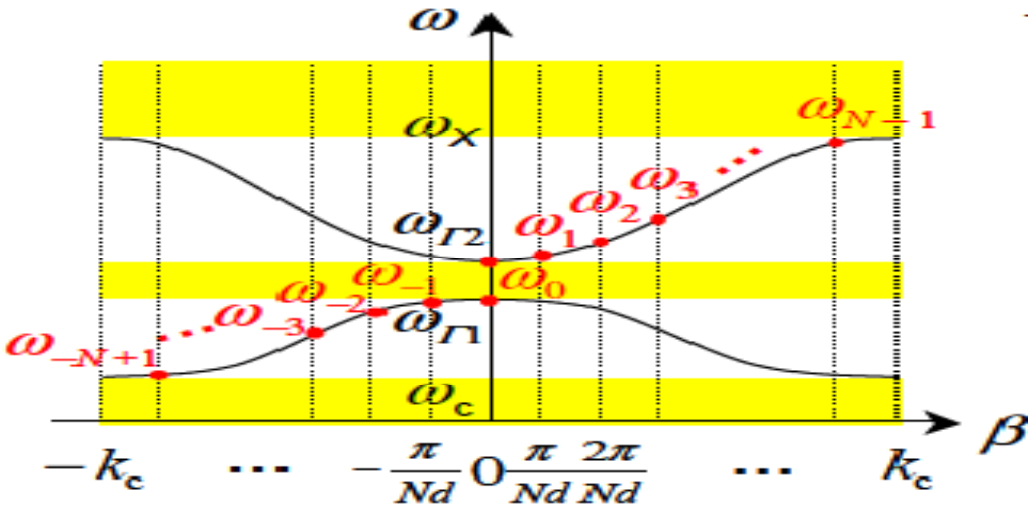

Figure 3-13 Dispersion diagram of the CRLH ZOR [74]

The input impedance of an open-ended CRLH ZOR when β→0 is given by:

$$Z_{in} = -jZ_0\frac{1}{\beta l} = -j\sqrt{\frac{Z'}{Y'}}\left(\frac{1}{-J\sqrt{Z'Y'}}\right)\frac{1}{l} = \frac{1}{Y'}\frac{1}{Nd} = \frac{1}{NY}$$

where $Z' = j\left(\omega L_L - \frac{1}{\omega C_R}\right)/d$, $Y' = j\left(\omega L_R - \frac{1}{\omega C_L}\right)/d$ and $Y = Y'd$

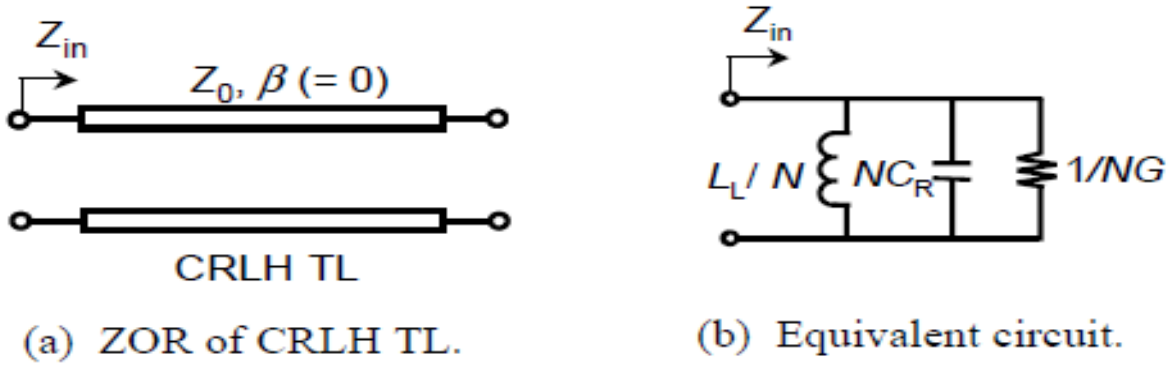

Figure 3-14 CRLH ZOR in resonance state[74]

The ZOR can be represented as shown in Figure 3-14. The equivalent circuit also shown is a LC anti-resonant tank circuit with inductance L_L/N and a capacitance of NC_R. Hence the resonant frequency of the ZOR can be written as:

$$\omega = \frac{1}{\sqrt{(L_L/N)NC_R}} = \frac{1}{\sqrt{L_L C_R}} = \omega_{sh}$$

This is a very interesting result as it shows that the resonant frequency of the ZOR is independent of the physical length l of the ZOR. It is dependent only on the resonant frequency shunt circuit with inductance L_L and capacitance C_R of the unit cell.

The unloaded Q factor of the ZOR is obtained from the equivalent circuit in Figure 3-14(b) as:

$$Q_0 = \frac{1/NG}{\omega_{sh}L/N} = \frac{1/G}{\omega_{sh}L} = \omega_{sh}(1/G)C$$

This is similar to the unloaded Q of the unit cell alone which indicates that the unloaded Q of the ZOR is independent of the number of unit cells [74].

3.5.1.3 Microstrip Implementation

Simulations and experiments have successfully been performed by [74] in order to validate the ZOR theory. An example of a 7-cell ZOR and a 1.5 cell ZOR implemented on microstrip lines is shown in Figure 3-15.

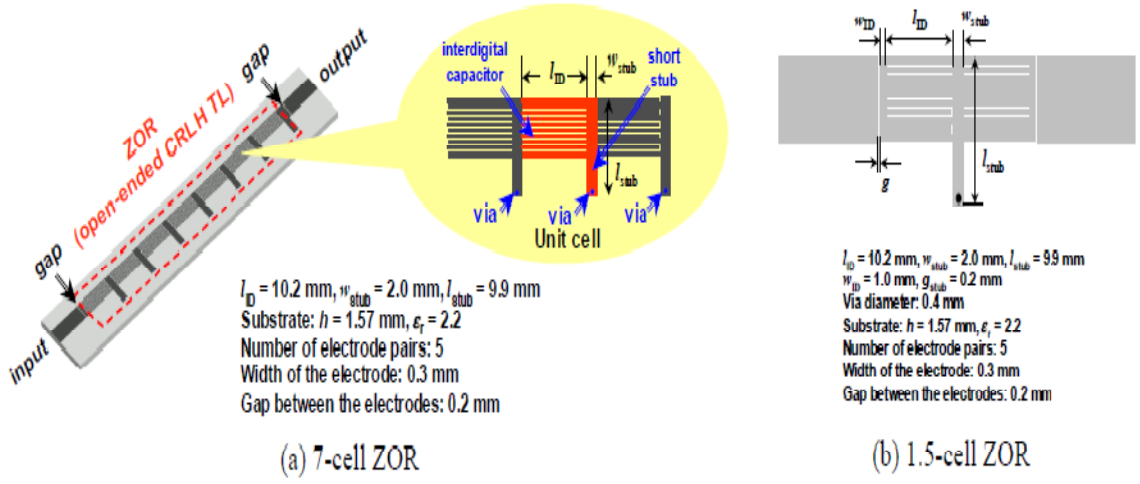

Figure 3-15 Microstrip realizations of CRLH ZOR [74]

The theoretical, simulated, and experimental results show a high level of agreement with each other thus validating the theory of the CRLH ZOR. The work done in [18] also verifies the validity of the ZOR theory by simulating a 2-cell ZOR at a resonance frequency of 2.4 GHz. The novel tag antenna designed in this thesis is an extension of the ZOR antenna discussed in this section. The design of this antenna is discussed in the next chapter.

Chapter 4

Design, Simulation, and Experimental testing of the Novel RFID Tag Antennas

The design of the novel tag antennas, based on the CRLH Zeroth Order Resonant (ZOR) antenna, is presented in this chapter. The designs are simulated using Agilent ADS Momentum and the results obtained are discussed and analyzed. The experimental testing of the antennas in an anechoic chamber is then demonstrated and the performance of the antenna is evaluated.

4.1 Antenna Design

The fundamental basis of the antenna designed is the CRLH ZOR, which was explained in the previous chapter. The design of the CRLH unit cell, which is the basic component of the antenna, is first explained.

4.1.1 The CRLH Unit Cell

The design of a CRLH unit cell has been explained in detail in [18]. The unit cell in [18] is designed to radiate at a frequency of 2.4 GHz. The same method has been used by Shi [76] to design a unit cell radiating at a frequency of 915 MHz. The unit cell used by the novel CRLH ZOR antennas is designed using the same procedure.

The substrate chosen for the design is FR4 substrate rather than Rogers Duroid 5880. The reason for this choice is that FR4 is more commercially available and involves a simpler fabrication process for small antennas. The drawback of using FR4 is that it has a higher dielectric constant and a higher tangent loss which leads to a reduction in antenna performance [77]. The target application of this thesis is RFID, wherein the antenna needs to be as small as possible and the

cost of tag production needs to be low. This dictates the choice of FR4 as the dielectric substrate of the antennas designed in this thesis.

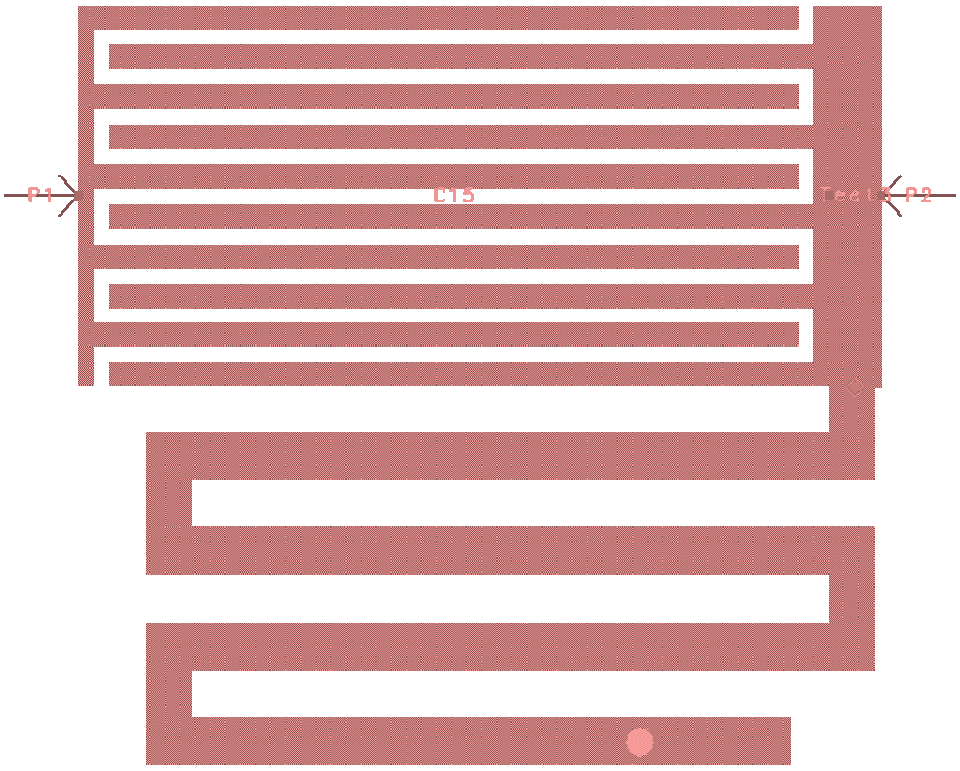

Figure 4-1 Unit Cell of CRLH ZOR Antenna

The unit cell consists of an interdigital capacitor and a shunt inductor which consists of a T-section and a meander-line, as shown in Figure 4-1. In the traditional CRLH ZOR [17], a shunt straight inductor is used which is replaced in this design by a meander-line inductor, which provides a larger inductance and reduces the size of the structure. A via connects the meander-line inductor to the ground plane. The parameters of the interdigital capacitor are shown in Figure 4-2 and the values used are provided in Table 4-1 .The dimensions of the T-section are 4.832 mm x 4.832 mm x 0.7 mm. The width of the meander-line is 0.6 mm and its total length is 39.5 mm. The diameter of the via connecting the meander-line to the ground plane is 0.35 mm.

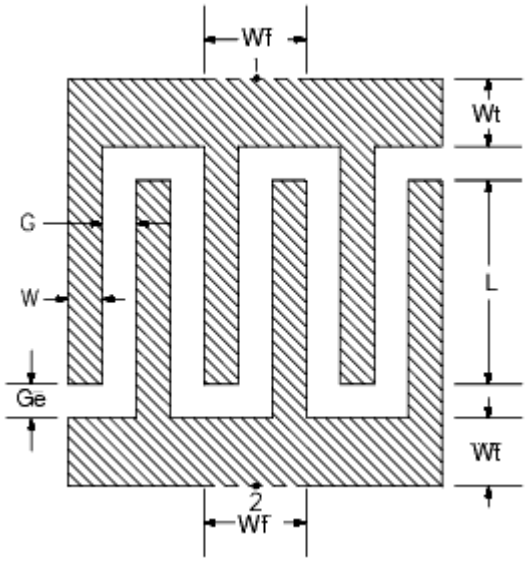

Figure 4-2 Interdigital Capacitor [78]

Parameter	Dimension (mm)
INTERDIGITAL CAPACITOR	
Finger Width (w)	0.3
Gap between fingers (G)	0.2032
Gap at the end of the fingers (Ge)	0.2032
Length of Overlapped region (L)	9.2
Number of finger pairs (Np)	5
Width of interconnect (Wt)	0.2
Width of the feed line (Wf)	4.8

Table 4-1 Parameters of the Interdigital Capacitor

The equivalent circuit of the unit cell is the same as that of the LC-based model of the CRLH TL, as shown in Figure 3-8(a). The parameters of the CRLH TL are extracted using the procedure specified in [18] and the resonant frequency is verified to be close to 915 MHz. The parameter extraction is performed by first obtaining the S parameters by simulating the entire structure (with a microstrip line attached on both sides of the unit cell) followed by the S parameters of the microstrip line. The ABCD matrix of the whole structure and that of the microstrip line are then

calculated from which the ABCD matrix of the unit cell is found. The S parameters of the unit cell are then calculated from the corresponding ABCD matrix, from which the phase constant and hence the transition frequency is found. The interdigital capacitor and the shunt inductor are then simulated separately to obtain their S parameters. The admittance matrix of the capacitor and the impedance matrix of the inductor are then found from the S parameters from which the values of the parameters are calculated.

This unit cell is the basic component of the 1-cell, 2-cell, and 4-cell CRLH ZOR antennas which are described in the next sections.

4.1.2 1-Cell CRLH ZOR Antenna

The single unit-cell CRLH ZOR antenna is shown in Figure 4-3. The unit cell described in the previous section is cascaded with a single input port through which the antenna is fed. The energy is coupled into the antenna through a gap. The dielectric substrate is FR4 which has a dielectric constant $\varepsilon_r = 4.4$ and a loss tangent of 0.002. The thickness of the substrate is 1.57 mm and the thickness of the copper is 35um. The design is simulated using Agilent ADS Momentum and the results are shown below. Figure 4-4 shows the S11 characteristics which gives the return loss for the antenna. Figure 4-5 shows the radiation characteristics of the antenna which include the 2-D and 3-D radiation patterns, the radiated power distribution, and the antenna parameters.

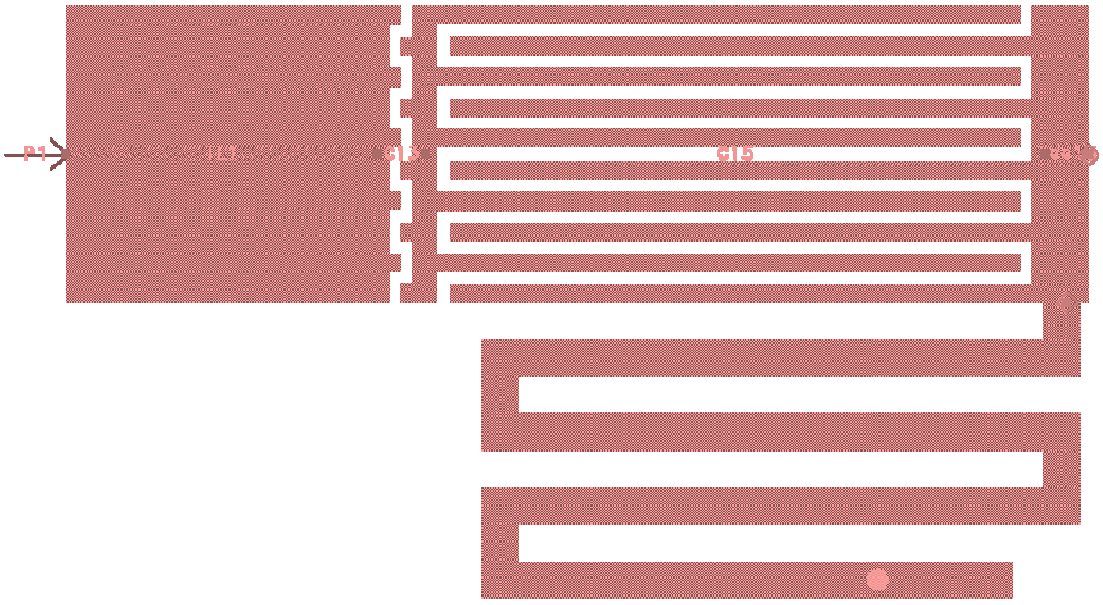

Figure 4-3 1- Unit Cell CRLH ZOR Antenna with a feed gap.

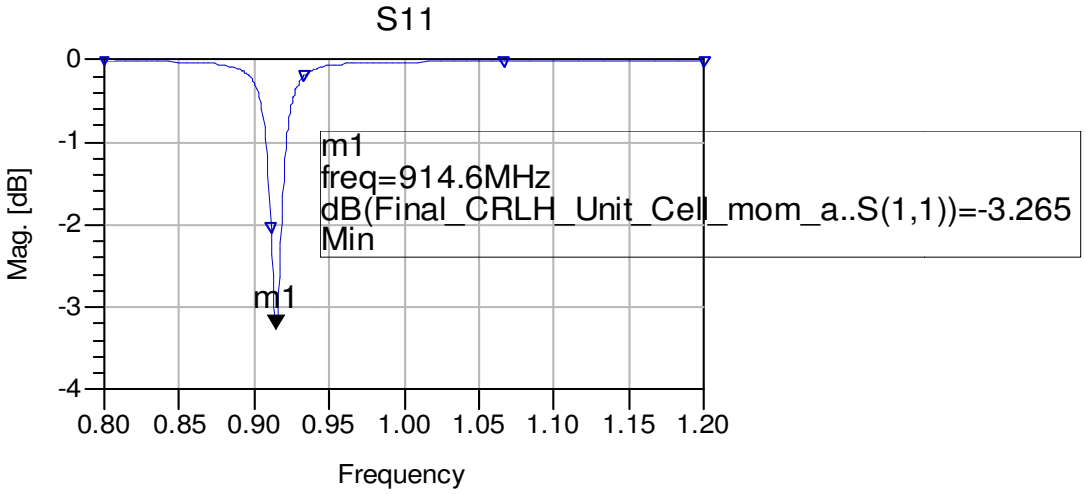

Figure 4-4 S11 characteristics of 1-cell CRLH ZOR Antenna

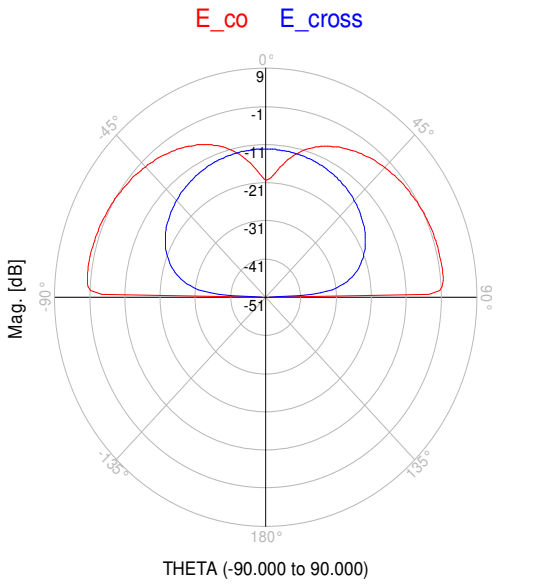

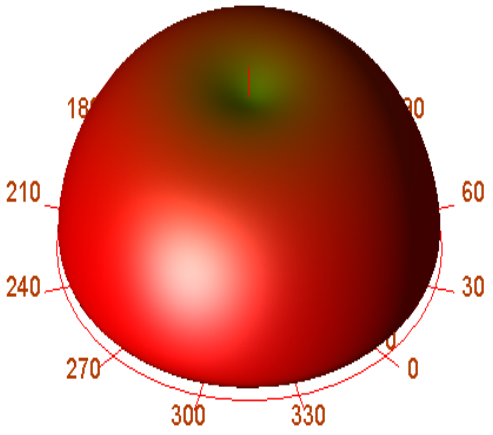

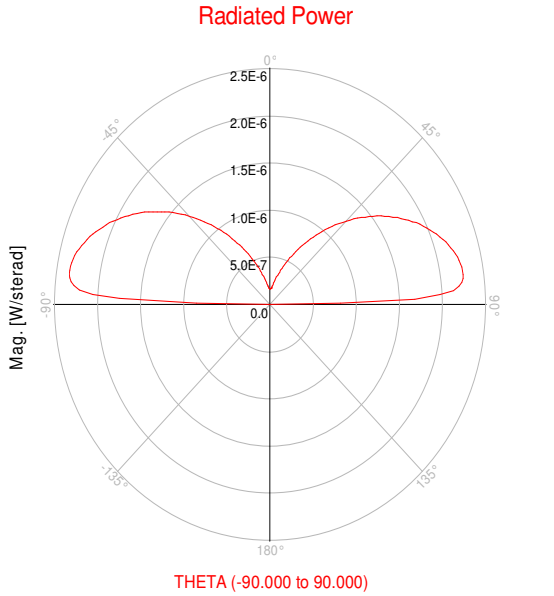

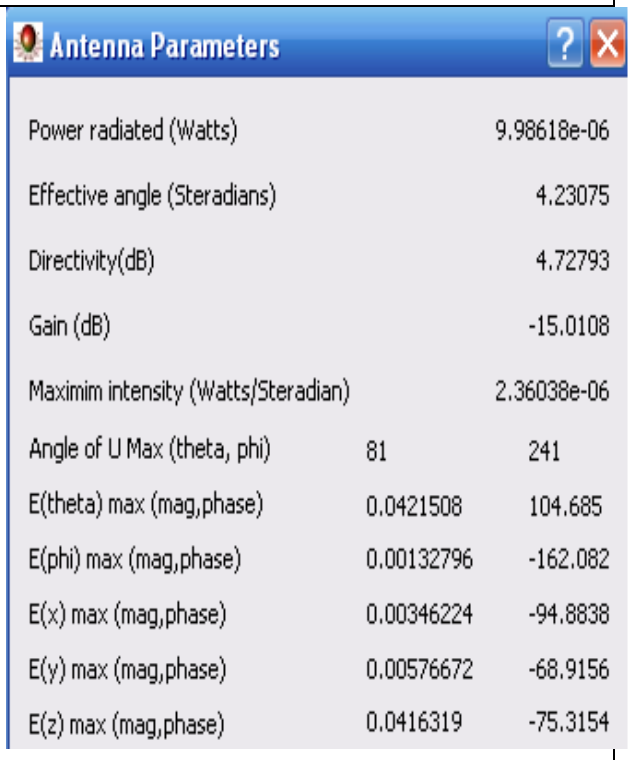

Figure 4-5 Radiation characteristics of 1-cell CRLH ZOR Antenna

It is evident from the results that the antenna is radiating at a frequency close to 915 MHz, which is the desired operating frequency. From the radiation pattern it can be inferred that the antenna is an end-fire antenna and not a broadside antenna, because the minimum radiation occurs at 90 degrees. This is also evident from the power radiation characteristics. The overall size of the antenna is 16.5 mm x 9.6 mm with an area of 158.4 sq. mm.

4.1.3 Multiple Cell (2-cell) CRLH ZOR Antenna

An additional unit cell is cascaded to the 1-cell ZOR antenna described in the previous section, as shown in Figure 4-6. According to the theory of the ZOR antenna described in the previous chapter, the change in the physical dimensions of the structure should not affect the resonant frequency of the antenna. The ADS Momentum simulation results are presented - the S11 characteristics are shown in Figure 4-7 and the radiation characteristics of the antenna are shown in Figure 4-8.

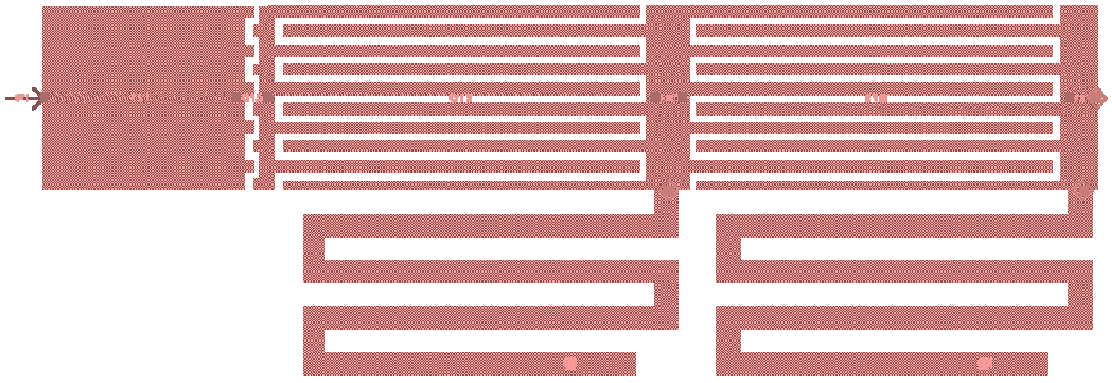

Figure 4-6 2-cell CRLH ZOR Antenna

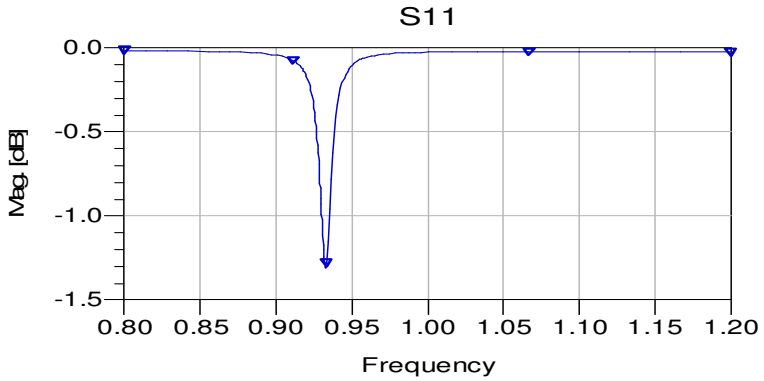

Figure 4-7 S11 characteristics of 1-cell CRLH ZOR Antenna

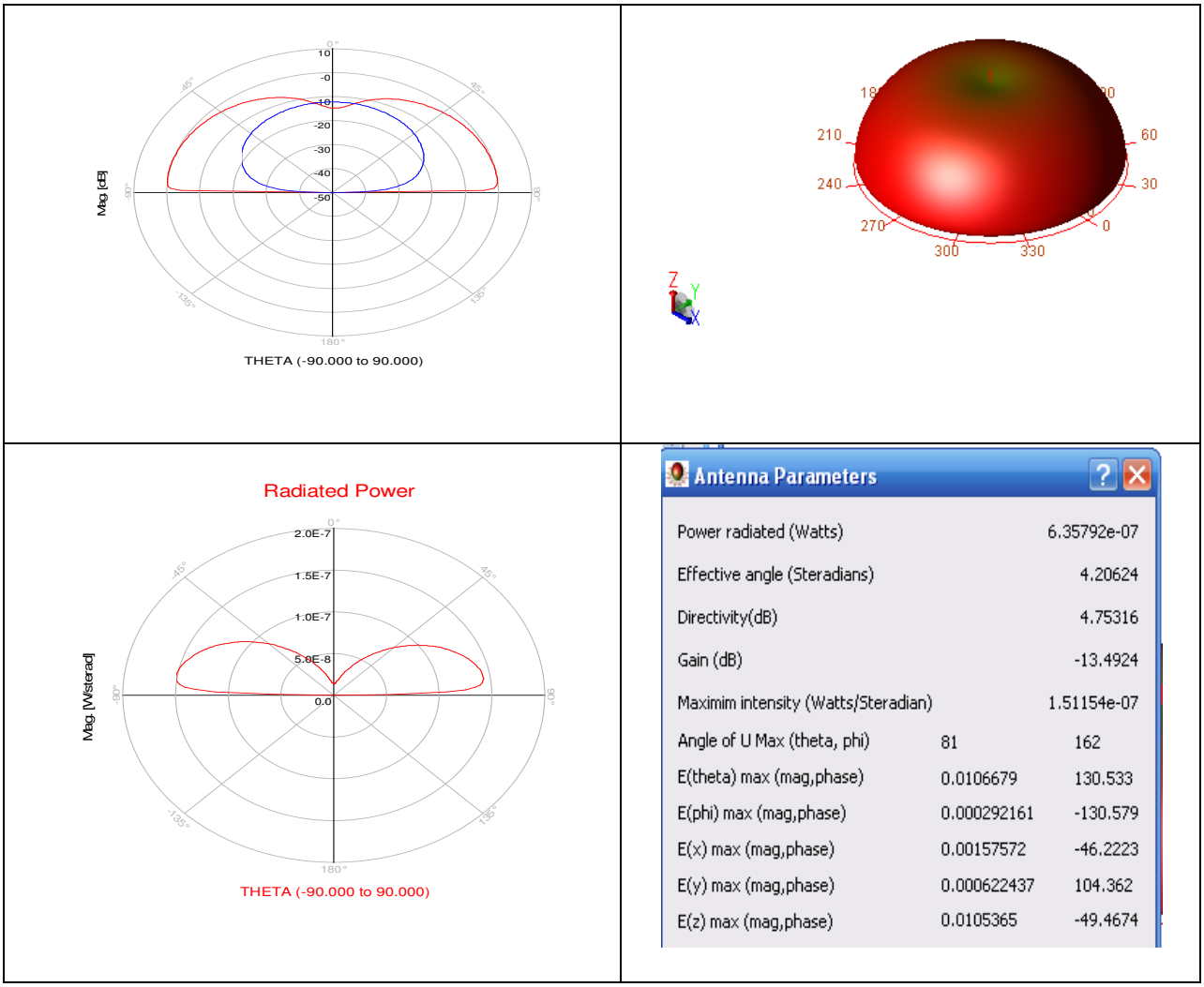

Figure 4-8 Radiation characteristics of the 2-cell CRLH ZOR Antenna

The simulation results verify the theory of the ZOR antenna because the resonant frequency is seen to be shifted only by a very small margin due to the addition of the extra cell. The radiation pattern indicates that this is also an end-fire antenna and the direction of radiation is similar to that of the 1-cell antenna. A slight increase in the directivity and gain is observed which implies a more efficient radiator. A decrease in the bandwidth of the antenna is also observed. The overall size of the 2-cell antenna is 27.2 mm x 9.6 mm with an area of 261.12 sq. mm.

4.1.4 Multiple Cell (4-Cell) CRLH ZOR Antenna

The 4-cell CRLH ZOR antenna is a cascade of 4 unit cells as shown in Figure 4-9. With the increase in the number of cells, although the antenna size increases, it is expected that the performance of the antenna will improve. The ADS Momentum simulation results are presented. S11 characteristics are shown in Figure 4-10 and the radiation characteristics of the antenna are shown in Figure 4-11.

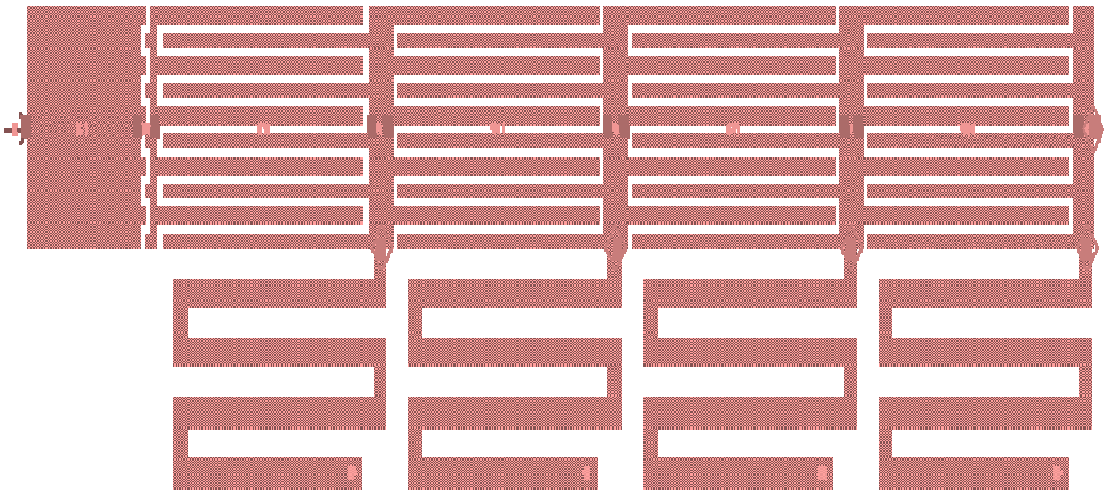

Figure 4-9 4-Cell CRLH ZOR Antenna

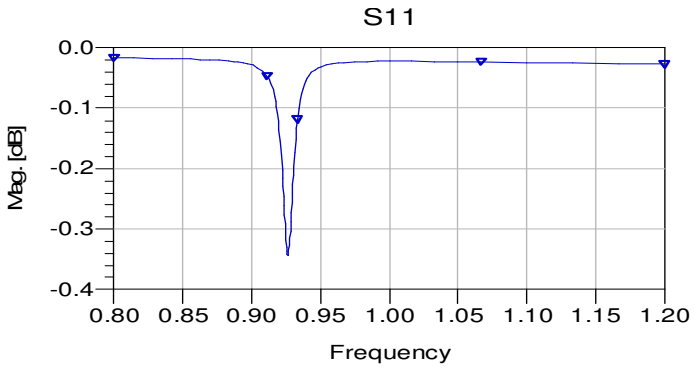

Figure 4-10 S11 characteristics of the 4-cell CRLH ZOR Antenna

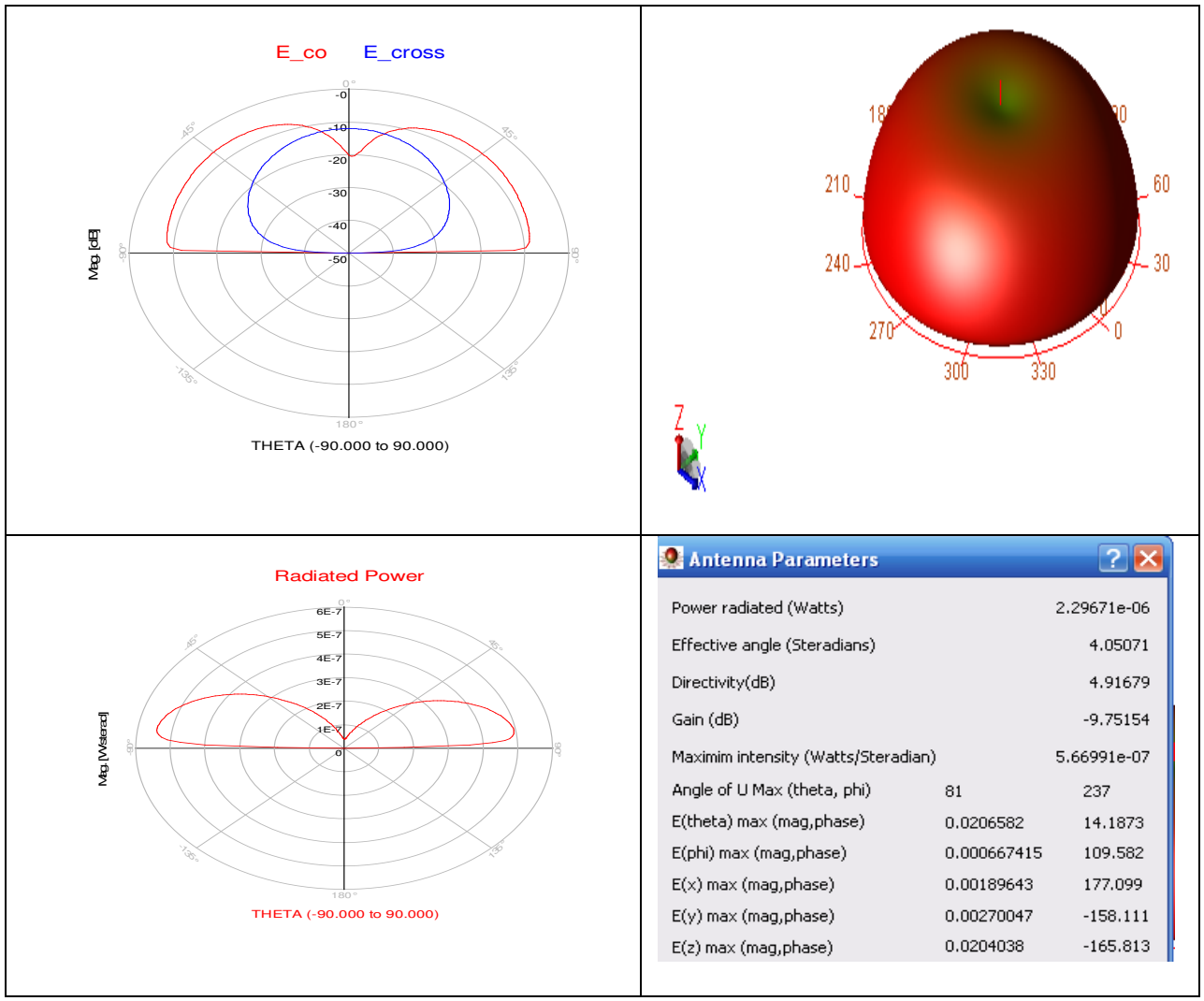

Figure 4-11 Radiation characteristics of the 4-cell CRLH ZOR Antenna

The 4-cell ZOR antenna shows a significant increase in the directivity and gain which implies that it is an even more efficient radiator than the 2-cell ZOR. It is interesting to note that the increase in the number of cells does not change the orientation of the antenna radiation. The radiation pattern of the 4-cell ZOR also indicates that the antenna is end-fire and radiates in the same direction as the previous configurations. The overall size of the antenna is 48mm x 9.6mm with an area of 460.8 sq. mm.

4.2 The Novel CRLH Tag Antennas

This section presents three novel CRLH ZOR antenna configurations which were designed and simulated using Agilent ADS Momentum. The simulation results for each antenna are presented and the performance of the antennas is compared with that of the traditional 2-cell and 4-cell antennas described in the previous section.

4.2.1 CRLH ZOR Antenna with 1 Unit Cell on each side (AUT1)

The traditional 2-cell CRLH ZOR antenna was seen in the previous section. In this novel CRLH ZOR antenna there are two unit cells present but are separated by a microstrip in-between, through which the antenna is fed. The layout of the antenna is shown in Figure 4-12 and a 3-dimensional view of the antenna is shown in Figure 4-13. The dielectric substrate is FR4 which has a dielectric constant $\varepsilon_r = 4.4$ and a loss tangent of 0.002. The thickness of the substrate is 1.57 mm and the thickness of the copper is 35um.

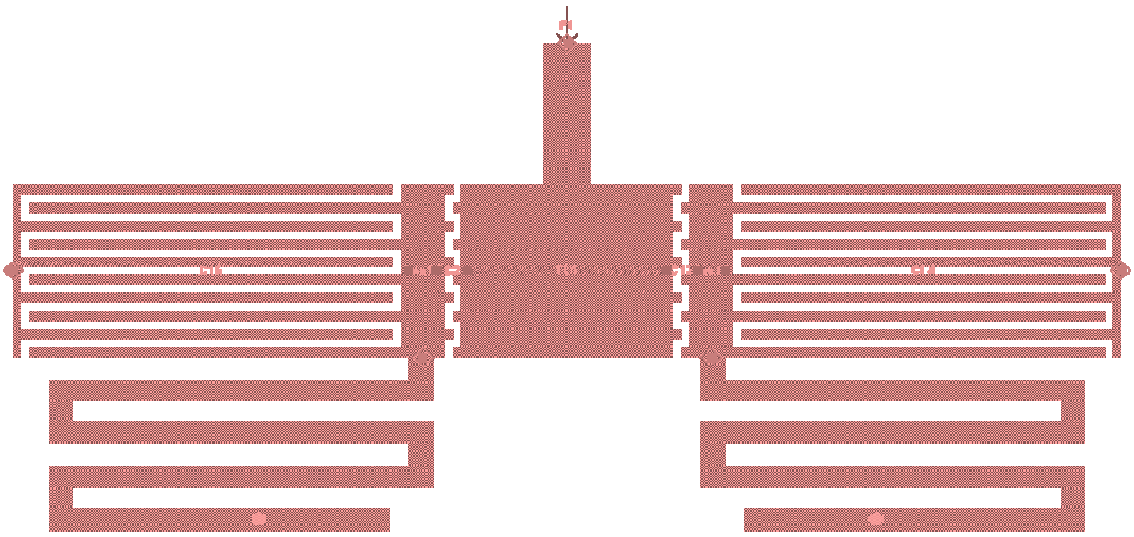

Figure 4-12 CRLH ZOR Antenna with 1-cell on each side

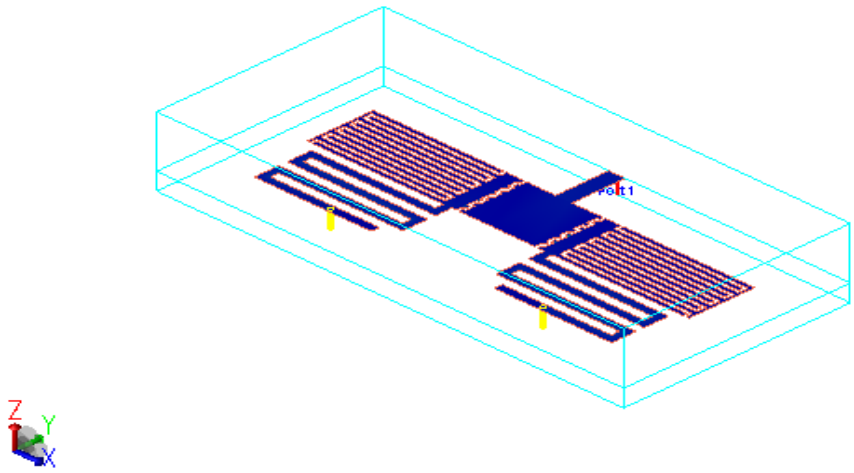

Figure 4-13 3-D view of the antenna

The antenna is simulated using Agilent ADS Momentum and the S11 characteristic is shown in Figure 4-14. The radiation characteristics of the antenna are shown in Figure 4-15. It can be seen from the S11 characteristics that the return loss of the antenna is -24.69 dB which is much lesser than the traditional 2-cell ZOR antenna discussed earlier. This indicates that this configuration is a much better radiator than the traditional 2-cell ZOR.

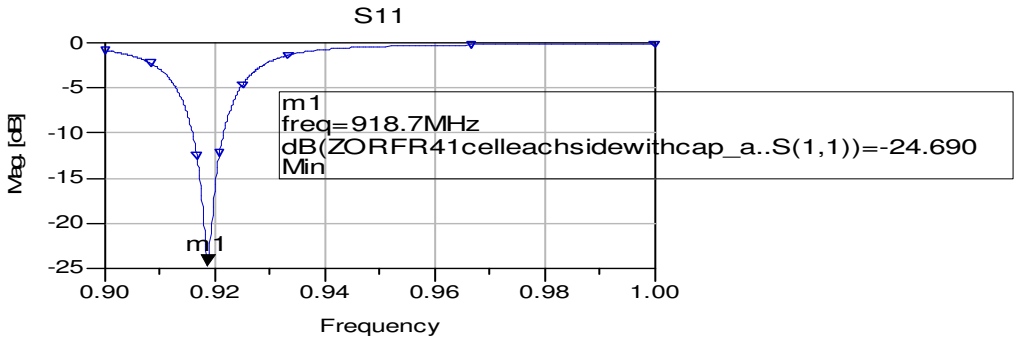

Figure 4-14 S11 characteristics of AUT1

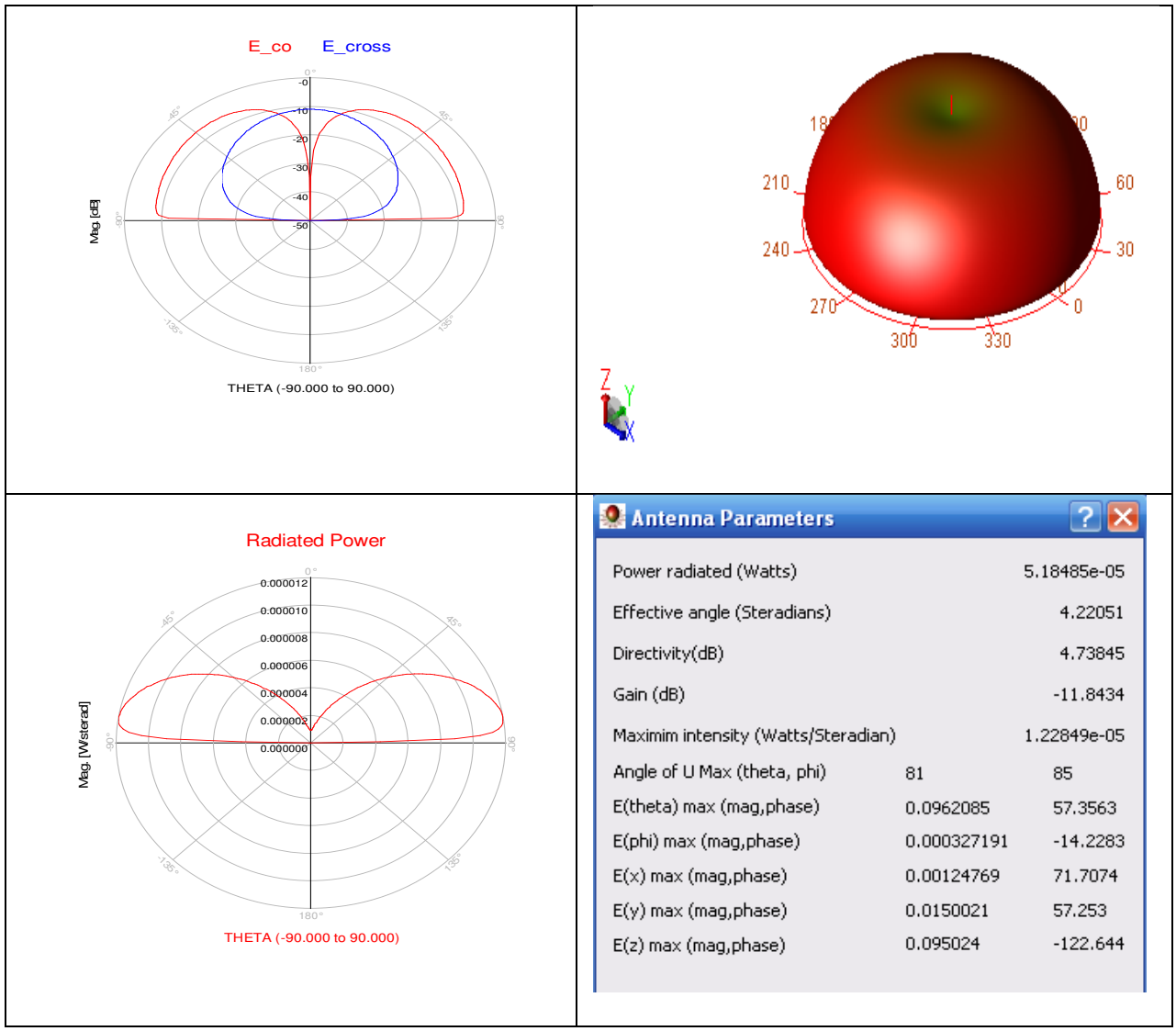

Figure 4-15 Radiation characteristics of AUT1

The radiation pattern of AUT1 shows that the radiation occurs in a similar direction as that of the traditional 2-cell ZOR. A significant increase is observed in the radiated power and gain which implies that the antenna is more efficient when compared to the traditional 2-cell ZOR. The main motivation behind this configuration is the application of this antenna as an RFID tag antenna. The size of the tag antenna needs to be as small as possible because of the space constraints in RFID applications. The RFID tag is constructed by attaching a chip to the tag antenna. In the traditional 2-cell ZOR antenna this implies that the chip attachment would be outside the structure and hence lead to an increase in the total size of the structure. In the novel configuration it is possible to attach the chip to the microstrip feed within the structure. Hence the total size of the structure is not increased which keeps the tag size small. The total size of the antenna is 28mm x 9.6mm with an area of 268.8 sq. mm.

4.2.2 CRLH ZOR Antenna with 2 Unit Cells on each side (AUT2)

The traditional 4-cell ZOR antenna was found to provide a better performance when compared to the 2-cell ZOR antenna. Hence the novel antenna described in the previous section is replicated with 2 unit cells on each side of the microstrip, as shown in Figure 4-16. The 3-dimensional view of the antenna is shown in Figure 4-17.

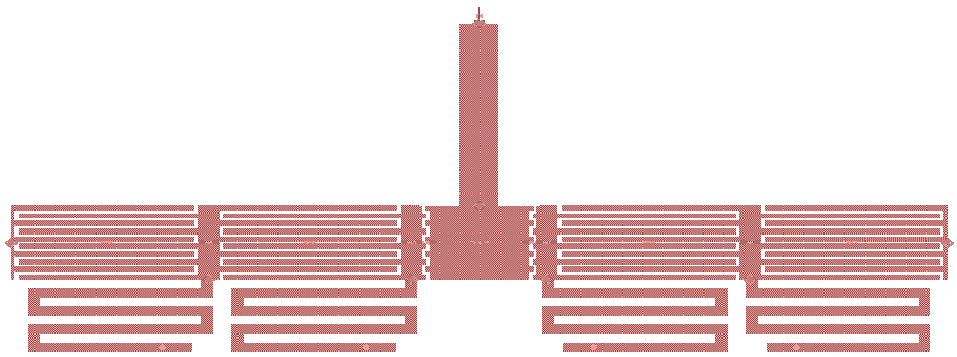

Figure 4-16 Layout of AUT2

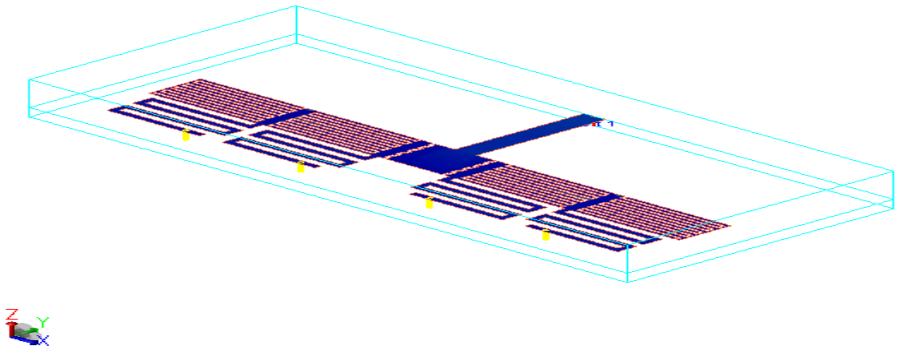

Figure 4-17 3-D view of AUT2

The antenna is simulated using Agilent ADS Momentum and the S11 plot is shown in Figure 4-18. The radiation characteristics of the antenna are shown in Figure 4-19. It can be seen from the S11 characteristics that the return loss of the antenna is -15 dB which is much lesser than that of the traditional 4-cell ZOR.

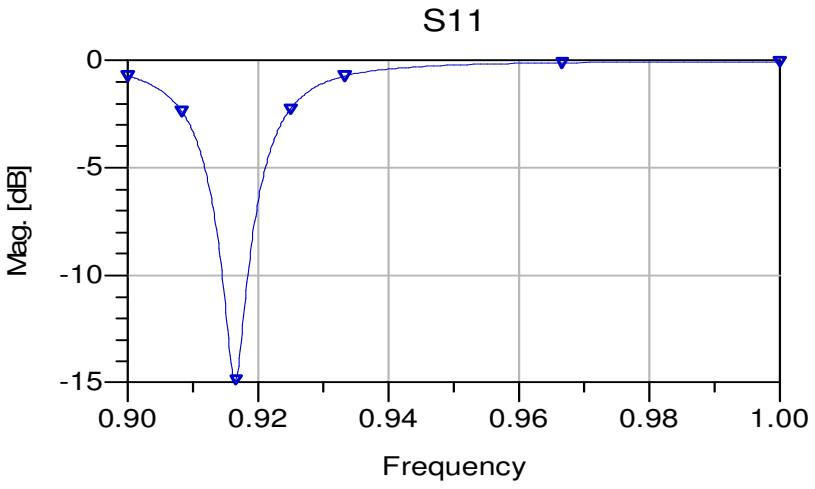

Figure 4-18 S11 plot of AUT2

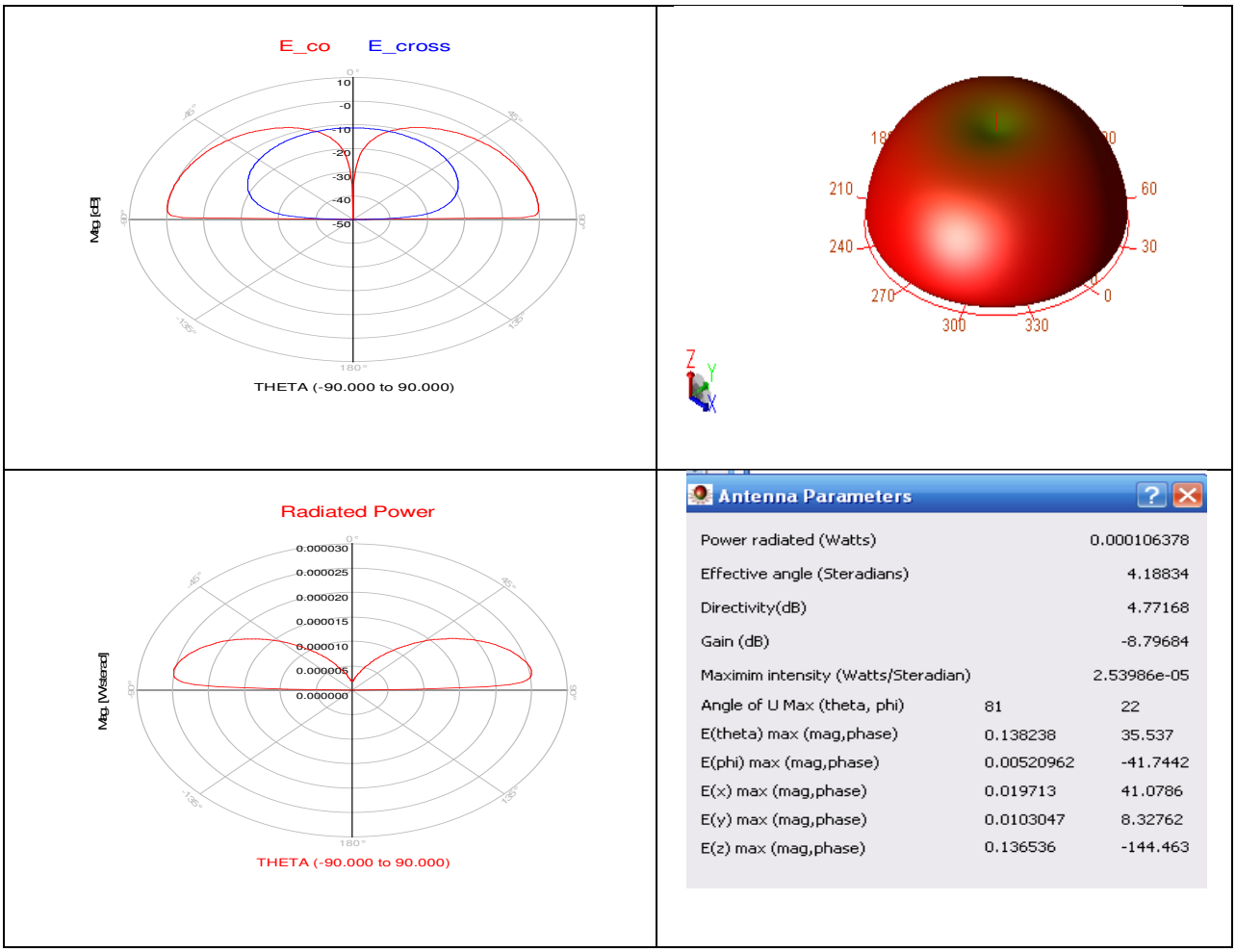

Figure 4-19 Radiation characteristics of AUT2

As in the previous cases it is evident from the radiation patterns that this configuration is also an end-fire antenna. The power radiated by this antenna is much higher than that of the traditional 4-cell ZOR antenna which makes it more ideal for use as a RFID tag antenna. The gain and directivity are also seen to be much higher. As in AUT1 the chip attachment for a tag can be made within the structure reducing the size of the tag. The overall size of the structure is 49.2mm x 9.6mm with an area of 472.32 sq. mm.

4.2.3 CRLH ZOR Antenna with 4 Unit Cells fed by a strip on top (AUT3)

Another novel configuration with 4 unit-cells is presented in this section. In this configuration the 4 unit-cells are cascaded in the same way as the traditional 4-cell ZOR antenna but the

energy is coupled through a horizontal microstrip on top of the unit-cells. The layout of this antenna is shown in Figure 4-20 and a 3-dimensional view of the antenna is shown in Figure 4-21. The dimension of the microstrip line on top is 42.8 mm x 3.1 mm. The motivation behind this configuration is that more energy will be coupled through the strip on top which will lead to better antenna performance. It is also seen to provide a better match with the 50 ohm feed line.

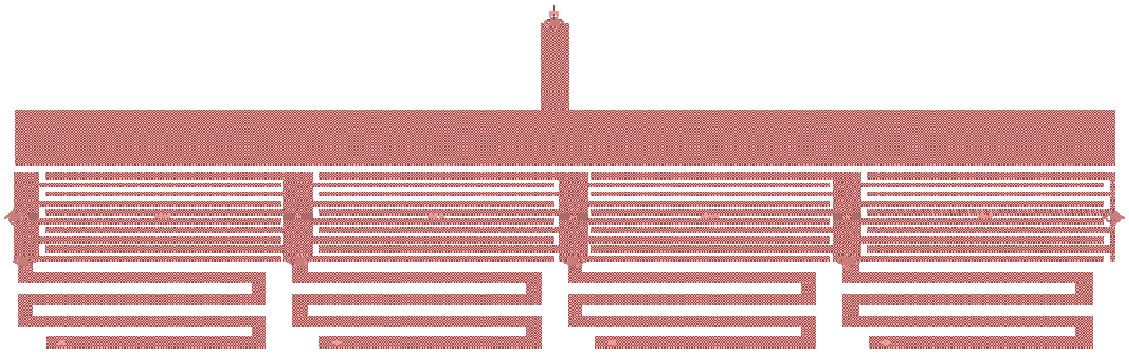

Figure 4-20 Layout of AUT3

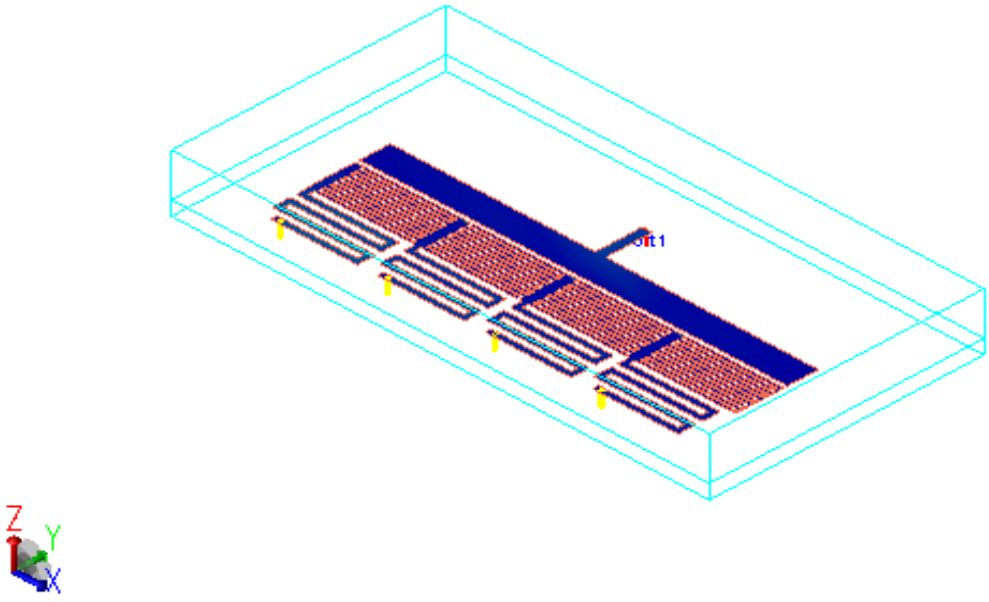

Figure 4-21 3-D view of AUT3

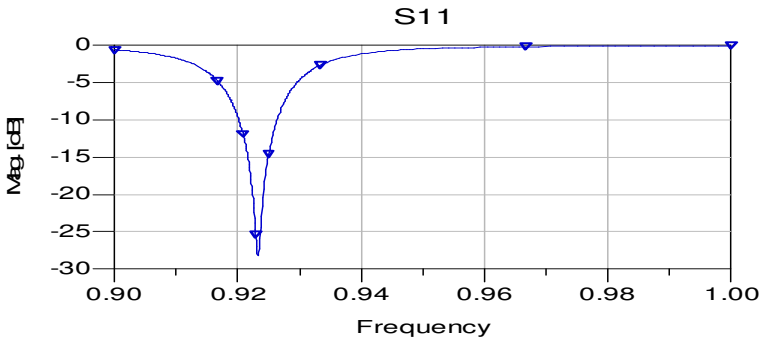

Figure 4-22 S11 plot of AUT3

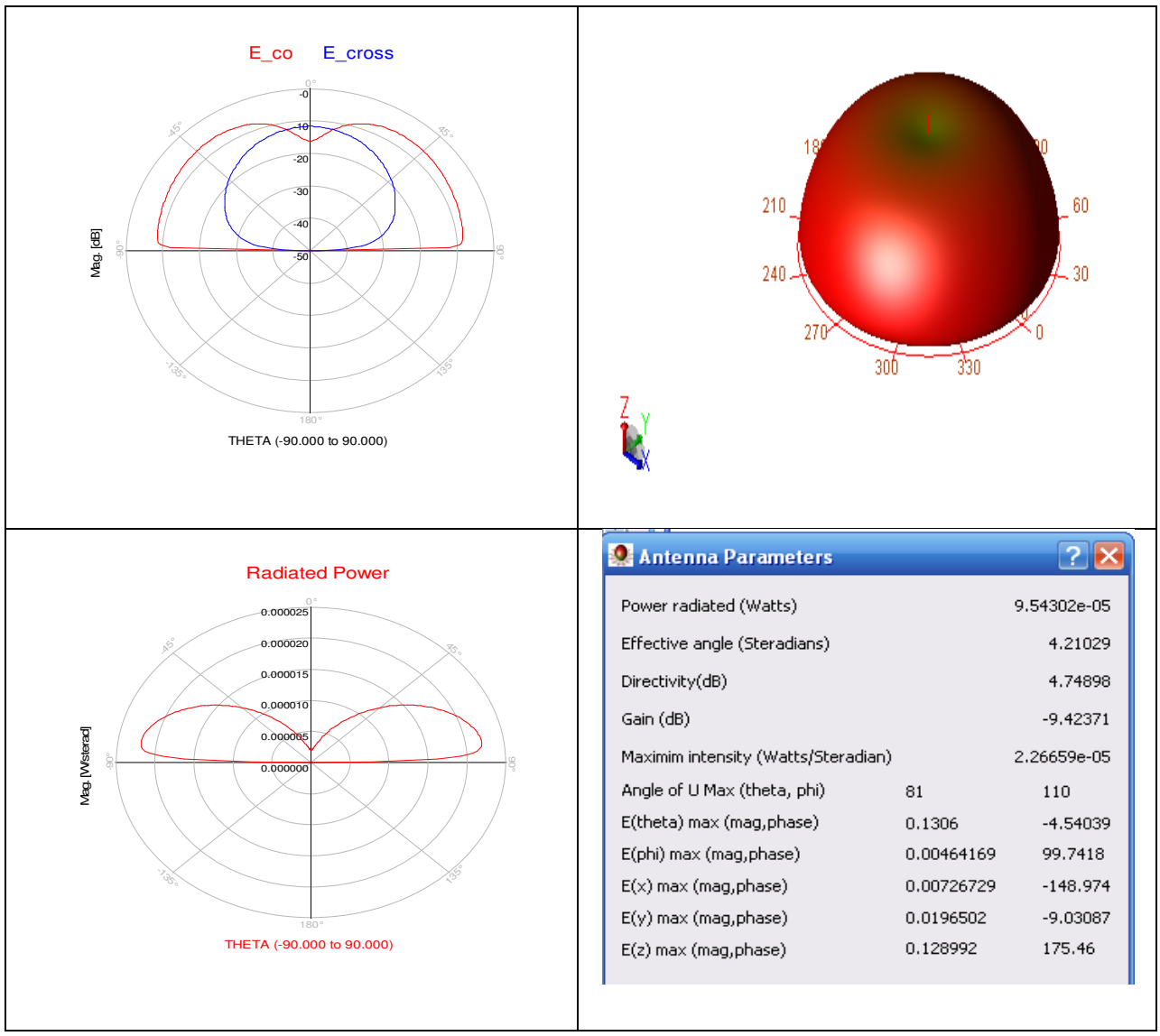

Figure 4-23 Radiation characteristics of AUT3

Figure 4-22 shows the S11 plot and Figure 4-23 shows the radiation characteristics of the antenna. It can be seen from the S11 characteristics that there is a very slight shift in the resonant frequency due to the increased number of unit cells as was seen in the traditional 4-cell ZOR antenna. It is also evident that the return loss of this antenna is much higher than any of the other configurations. The directivity and gain of AUT3 is equivalent to that of AUT2 but much higher than that of the traditional 4-cell ZOR antenna. The overall size of the structure is 42.8mm x 13.1mm with an area of 560.68 sq. mm.

4.2.4 Novel and Traditional CRLH ZOR Antenna Comparison

The results obtained from the ADS simulations for the traditional and novel CRLH ZOR antennas are summarized in

Table **4-2**. It can be seen from the table that the novel antennas perform much better than the traditional antennas.

Antenna	Return Loss (dB)	Power Radiated (Watts)	Gain (dB)	Radiation Orientation	Size (mm)
1-Cell CRLH ZOR	-3.265	9.99e-06	-15	End-fire	16.5 x 9.6
2-Cell CRLH ZOR	-1.3	6.4e-07	-13.5	End-fire	27.2 x 9.6
4-Cell CRLH ZOR	-0.34	2.3e-06	-9.75	End-fire	48 x 9.6
AUT1	-24.69	5.1e-05	-11.8	End-fire	28 x 9.6
AUT2	-15	1e-04	-8.8	End-fire	49.2 x 9.6
AUT3	-28	9.5e-05	-9	End-fire	42.8 x 13.1

Table 4-2 Summary of simulation results

4.3 Performance Comparison with a Rectangular Patch Antenna

A standard rectangular patch antenna is designed to radiate at 915 MHz and the simulation results are compared with those of the novel CRLH ZOR antennas.

4.3.1 Rectangular Patch Antenna

The most popular microstrip antenna is the simple rectangular patch antenna. A rectangular patch antenna with inset feed is designed as a reference antenna to evaluate the performance of the novel CRLH ZOR antennas. The design procedure described in Chapter 2 is used to design the patch antenna at 915 MHz. The layout of the antenna is shown in Figure 4-24. The antenna is simulated using ADS Momentum and the S11 characteristic is shown in Figure 4-25. The radiation characteristics are shown in Figure 4-26. The size of the rectangular patch is 104.6mm x 78mm with an area of 8158.8 sq. mm.

Figure 4-24 Patch antenna layout

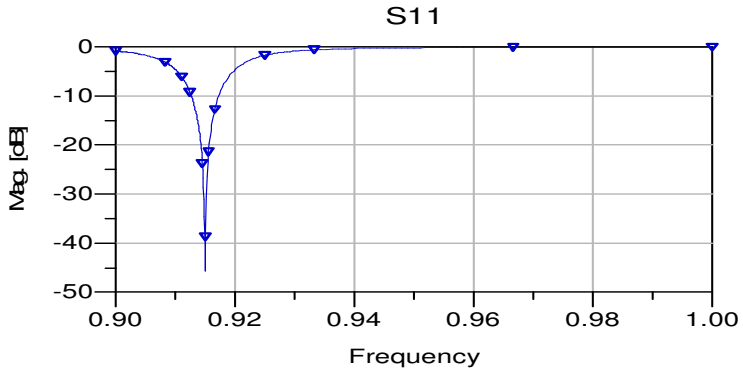

Figure 4-25 S11 plot of the patch antenna

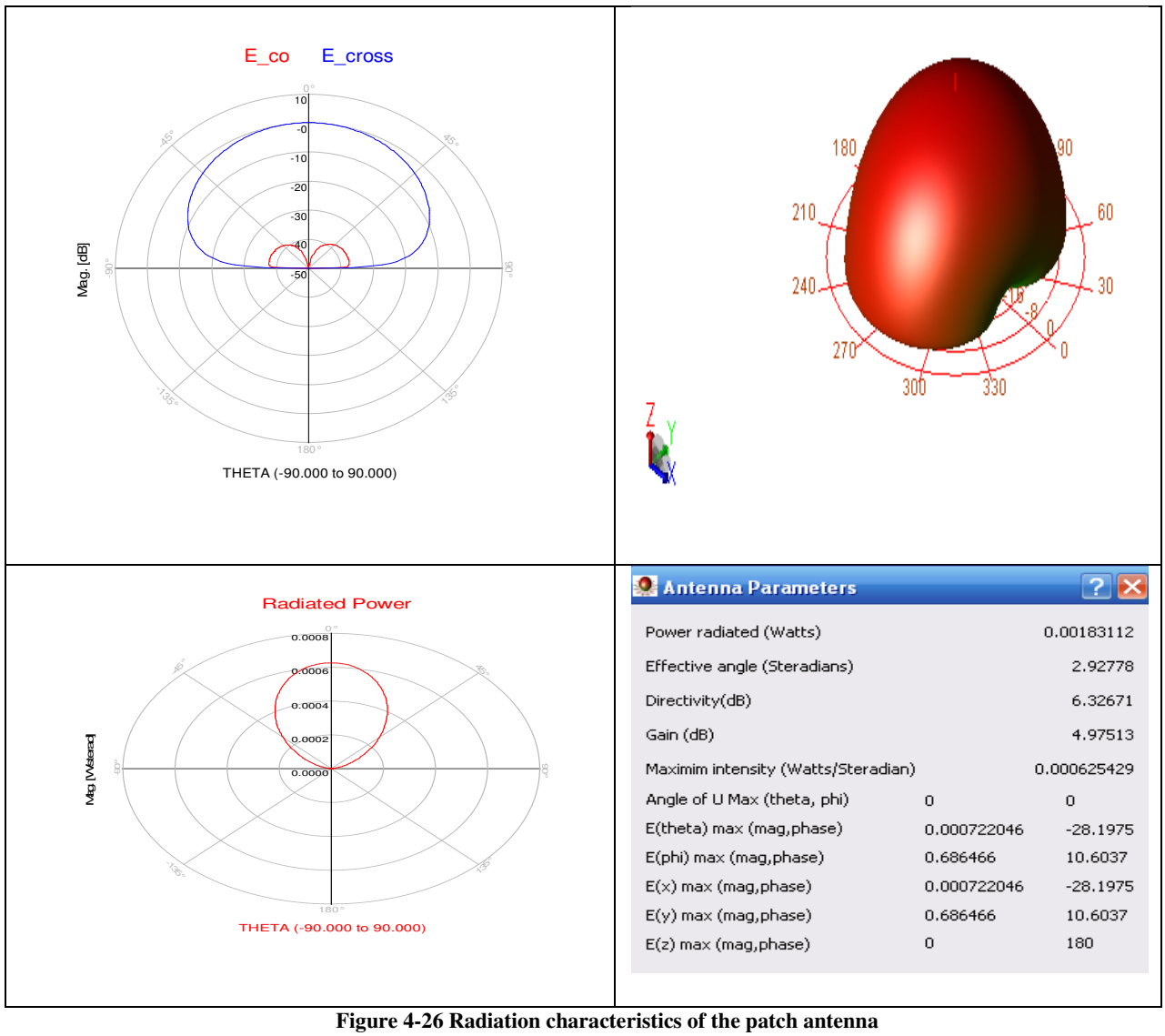

Figure 4-26 Radiation characteristics of the patch antenna

It can be seen from the S11 characteristics that the patch antenna has an excellent return loss of -45 dB. The radiation pattern shows that the direction of maximum radiation is normal to the plane of the antenna which implies that the patch antenna is a broadside radiator rather than an end-fire radiator. The power radiated is close to 1.8 mW and the gain and directivity are also quite high. As expected, the results indicate that the simple rectangular patch antenna exhibits very good radiation characteristics.

4.3.2 Comparison of Results

The simulation results of the three novel CRLH ZOR antennas and the rectangular patch antenna are summarized in Table 4-3.

Parameter	AUT1	AUT2	AUT3	Patch
Antenna Area (sq. mm)	268.8	472.32	560.68	8158.8
Resonant Frequency (MHz)	918.7	918	922	915
Return Loss (dB)	-24.69	-15	-28	-45
Radiated Power (Watts)	5.2e-05	1e-04	9.5e-05	1.8e-03
Directivity (dB)	4.7	4.77	4.75	6.3
Gain (dB)	-11.8	-8.8	-9.4	4.9
Radiation Pattern	End-Fire	End-Fire	End-Fire	Broadside

Table 4-3 Comparison of the novel CRLH ZOR antennas and the patch antenna

It is evident from Table 4-3 that the biggest differentiator between the novel CRLH ZOR antennas and the rectangular patch antenna is the size of the antenna. The area of the patch antenna is 30 times that of AUT1, 17 times that of AUT2, and 15 times that of AUT3. This is the major factor which prevents the use of the rectangular patch antenna in RFID applications. The other difference that is evident is that while the patch antenna is a broadside radiator, the CRLH

antennas are end-fire radiators. This can be used as an advantage in certain RFID applications such as pallet tags.

The power radiated by AUT2 is higher than AUT1 and AUT3, and is comparable with the power radiated by the patch antenna. The directivity of the novel antennas is around 4.7 dB which is comparable to that of the patch antenna. The drawback of the novel CRLH ZOR antennas is the low antenna gain and radiated power compared to the patch antenna. This implies that they are not suitable for long-range applications and can only be used for short-range applications. However this drawback is made up by the reduction in the size of the antenna which makes them suitable for short-range RFID applications.

4.4 Effect of Substrate and Metal properties on Antenna performance

The effect of the substrate and metal properties on the performance of the novel antennas designed is explored in this section. Three parameters – substrate height (h), metal thickness (t), and dielectric loss tangent (δ) - are varied and the effect of the variation on the antenna performance is analyzed. Simulations are performed for the three cases and the results are compared.

4.4.1 Substrate Height (h)

The simulations are performed for three values of substrate height: 1.57mm, 1mm, and 0.75mm. The other parameters are not varied – Dielectric material is FR4 (ε_r=4.4 and δ=0.002) and the copper thickness is 35um. As the substrate height is reduced it is noted that the resonant frequency decreases. In order to maintain the desired resonance frequency the length of the meander line is accordingly decreased. The results obtained for AUT1, AUT2, and AUT3 are shown in Table 4-4, Table 4-5, and Table 4-6.

Parameter	AUT1	AUT2	AUT3
Resonant Frequency (MHz)	918.7	918	922
Return Loss (dB)	-24.69	-15	-28
Radiated Power (Watts)	5.2e-05	1e-04	9.5e-05
Directivity (dB)	4.7	4.77	4.75
Gain (dB)	-11.8	-8.8	-9.4

Table 4-4 Results with h=1.57mm

Parameter	AUT1	AUT2	AUT3
Resonant Frequency (MHz)	919.8	919	917.7
Return Loss (dB)	-7.85	-5.4	-19.7
Radiated Power (Watts)	1.82e-05	3.16e-05	1.8e-04
Directivity (dB)	4.90	5.03	5.75
Gain (dB)	-14.79	-11.76	-5.53

Table 4-5 Results with h=1mm

Parameter	AUT1	AUT2	AUT3
Resonant Frequency (MHz)	913.7	912.4	911.8
Return Loss (dB)	-4.2	-2.67	-7.48
Radiated Power (Watts)	8.4e-06	8.57e-06	4.09e-05
Directivity (dB)	4.86	5.00	4.86
Gain (dB)	-16.83	-14.03	-7.75

Table 4-6 Results with h=0.75mm

As the height of the substrate decreases, the following observations can be made from the results:

- There is an increase in the return loss for all 3 antennas.
- The directivity is seen to be slightly higher when the substrate height is 1mm.
- There is a significant decrease in the radiated power and the gain of AUT1 and AUT2 whereas AUT3 shows an increase in power and gain when the height is 1mm.

4.4.2 Metal (Copper) Thickness (t)

Simulations are carried out with copper thicknesses of 17um, 35um, and 70um. The other parameters are not varied - Dielectric material is FR4 (ε_r=4.4 and δ=0.002) and the copper thickness is 1.57mm. The results obtained for AUT1, AUT2, and AUT3 are tabulated and analyzed.

Parameter	AUT1	AUT2	AUT3
Resonant Frequency (MHz)	915.6	916.7	923.6
Return Loss (dB)	-24.19	-16.49	-24.057
Radiated Power (Watts)	5.6e-05	1.1e-04	9.9e-05
Directivity (dB)	4.7	4.79	4.74
Gain (dB)	-11.7	-8.6	-9.2

Table 4-7 Results with t=17um (1/2 oz Copper)

Parameter	AUT1	AUT2	AUT3
Resonant Frequency (MHz)	918.7	918	922
Return Loss (dB)	-24.69	-15	-28
Radiated Power (Watts)	5.2e-05	1e-04	9.5e-05
Directivity (dB)	4.7	4.77	4.75
Gain (dB)	-11.8	-8.8	-9.4

Table 4-8 Results with t=35um (1 oz Copper)

Parameter	AUT1	AUT2	AUT3
Resonant Frequency (MHz)	915.2	916.7	923.2
Return Loss (dB)	-19.9	-14.23	-32.594
Radiated Power (Watts)	5.1e-05	1e-04	9.2e-05
Directivity (dB)	4.73	4.79	4.75
Gain (dB)	-12	-8.9	-9.6

Table 4-9 Results with t=70um (2 oz Copper)

It can be seen from the results that the variation in the thickness of the copper metallization layer does not have much of an impact on the performance of the antenna. There is only a slight decrease in the return loss while all the other parameters are not affected by the change in copper thickness.

4.4.3 Dielectric Loss Tangent

The simulations are carried out with three values of the dielectric loss tangent – 0 (Ideal case), 0.0009 (Duroid), and 0.002 (FR4). The results obtained for AUT1, AUT2, and AUT3 are tabulated and analyzed.

Parameter	AUT1	AUT2	AUT3
Resonant Frequency (MHz)	919	916.4	923.3
Return Loss (dB)	-36.6	-23.6	-17.09
Radiated Power (Watts)	6.7e-05	1.3e-04	1.1e-04
Directivity (dB)	4.72	4.82	4.73
Gain (dB)	-10.9	-7.85	-8.56

Table 4-10 Results with δ = 0

Parameter	AUT1	AUT2	AUT3
Resonant Frequency (MHz)	919	916.4	923.3
Return Loss (dB)	-29.5	-18.66	-20.77
Radiated Power (Watts)	6e-05	1.2e-04	1e-04
Directivity (dB)	4.72	4.82	4.74
Gain (dB)	-11.4	-8.3	-8.98

Table 4-11 Results with δ = 0.0009

Parameter	AUT1	AUT2	AUT3
Resonant Frequency (MHz)	918.7	918	922
Return Loss (dB)	-24.69	-15	-28
Radiated Power (Watts)	5.2e-05	1e-04	9.5e-05
Directivity (dB)	4.7	4.77	4.75
Gain (dB)	-11.8	-8.8	-9.4

Table 4-12 Results with δ = 0.002

As the dielectric loss tangent is decreased, the following observations are made:

- There is no impact on the resonant frequency of the antennas.
- There is a significant decrease in the return loss of the antennas.
- There is a slight increase in the radiated power.
- The gain of the antennas increases.

Hence it can be concluded from the above observations that a dielectric material with a lesser loss tangent will provide a better overall performance. However dielectric materials which have a very low loss tangent are more expensive and will not be suitable for cost-effective applications.

4.5 Experimental Verification

The novel CRLH ZOR antennas – AUT1, AUT2, and AUT3 – are fabricated on a FR4 substrate and experiments are performed to evaluate the performance of the antennas. The antennas are first tested using a Vector Network Analyzer (VNA) to check the resonant frequency and the return loss. The radiation characteristic of the antennas is then tested in an Anechoic Chamber and the results are presented. The VNA and the anechoic chamber are shown in Figure 4-27.

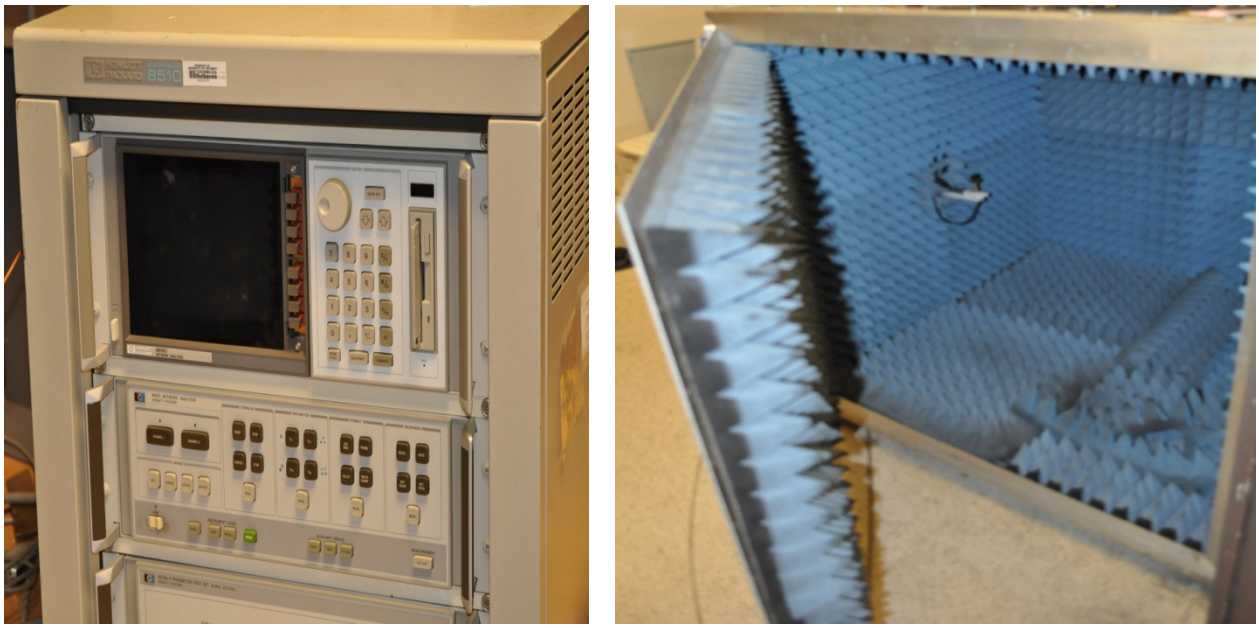

Figure 4-27 Vector Network Analyzer (HP8510) and Anechoic Chamber

4.5.1 AUT1 – Testing Results

The novel CRLH ZOR antenna with 1-unit cell on each side is fabricated on a 1.57mm thick FR4 substrate. The weight of the copper for the top and ground layers is 1 oz (35um). The size of the ground plane is taken to be more than the size of the antenna by 6 times the substrate height. Figure 4-28 shows a photograph of the fabricated antenna placed next to a cent for size comparison.

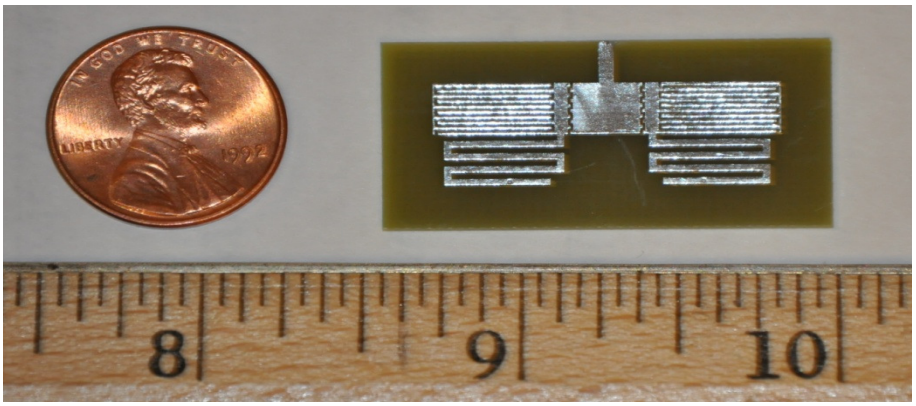

Figure 4-28 Photograph of AUT1

The antenna is first tested using the Vector Network Analyzer (VNA) to check the frequency of resonance and the return loss. The VNA is initially calibrated in the frequency band of interest, which is 900 MHz to 1000 MHz. Single-port mode of operation is chosen and the antenna is connected to the VNA using the coaxial cable connector. The S11 data is collected from the VNA and the graph plotted is shown in Figure 4-29. It can be seen from the S11 plot that the frequency of resonance is 938 MHz and the return loss is -9 dB .

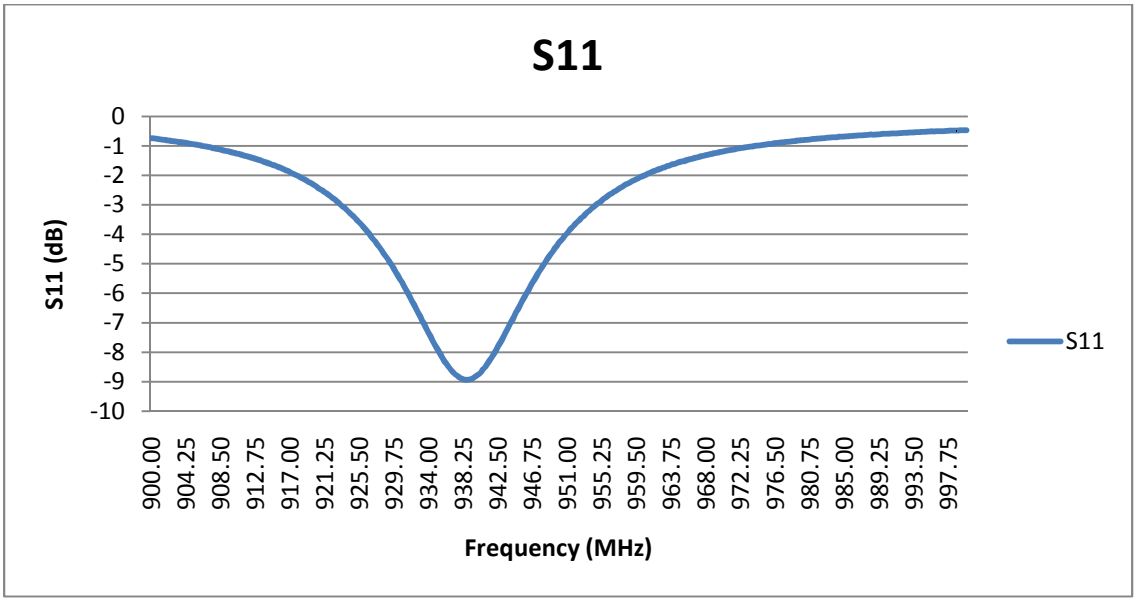

Figure 4-29 Measured S11 - AUT1

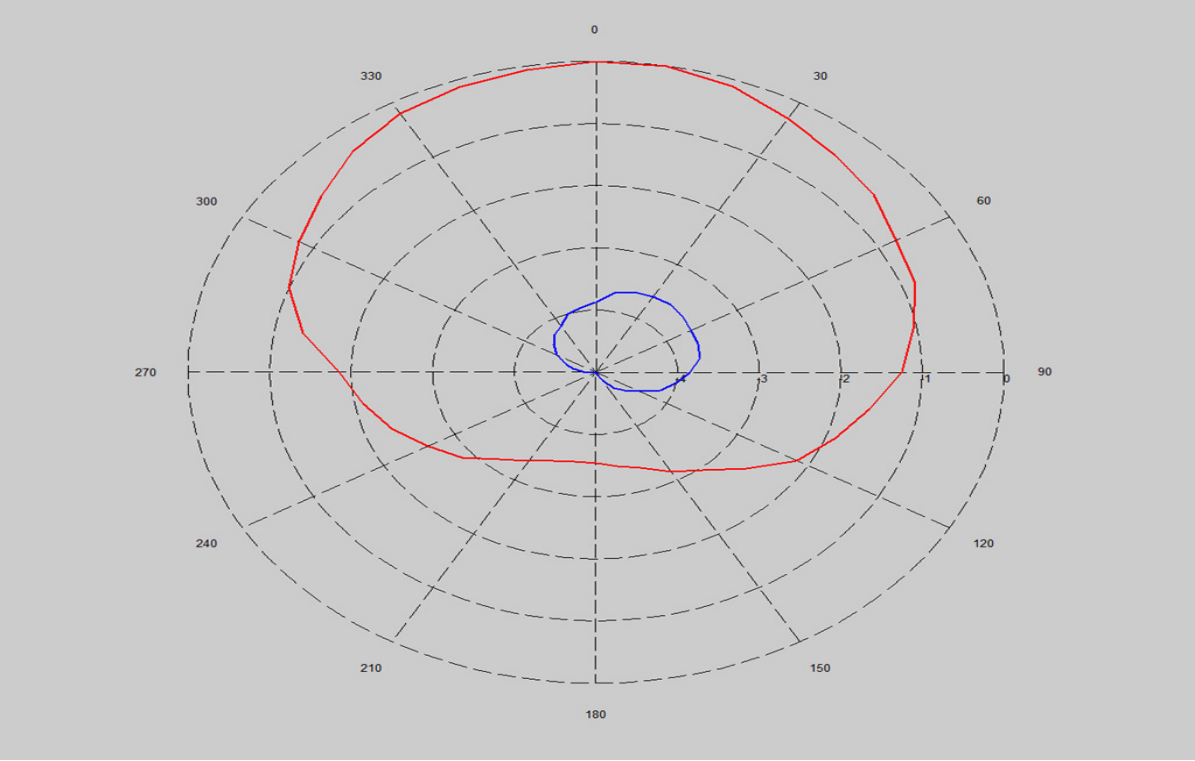

Figure 4-30 Measured radiation plot of AUT1

The radiation of the antenna is then tested in an anechoic chamber. Two tests are performed; one with the test and reference antennas parallel to each other and the other with the test and reference antennas perpendicular to each other. The antenna is rotated along the feed line and the power received at each step is recorded. The resultant plot of the power over a complete 360 degree rotation provides an insight into the radiation characteristics of the antenna. The polar plots for both test cases are shown in Figure 4-30.

4.5.2 AUT2 – Testing Results

The novel CRLH ZOR antenna with 2 cells on each side (AUT2) is fabricated on a FR4 substrate. The thickness of the substrate is 1.57mm and the copper thickness is 35 um. A photograph of the fabricated antenna placed next to a quarter is shown in Figure 4-31.

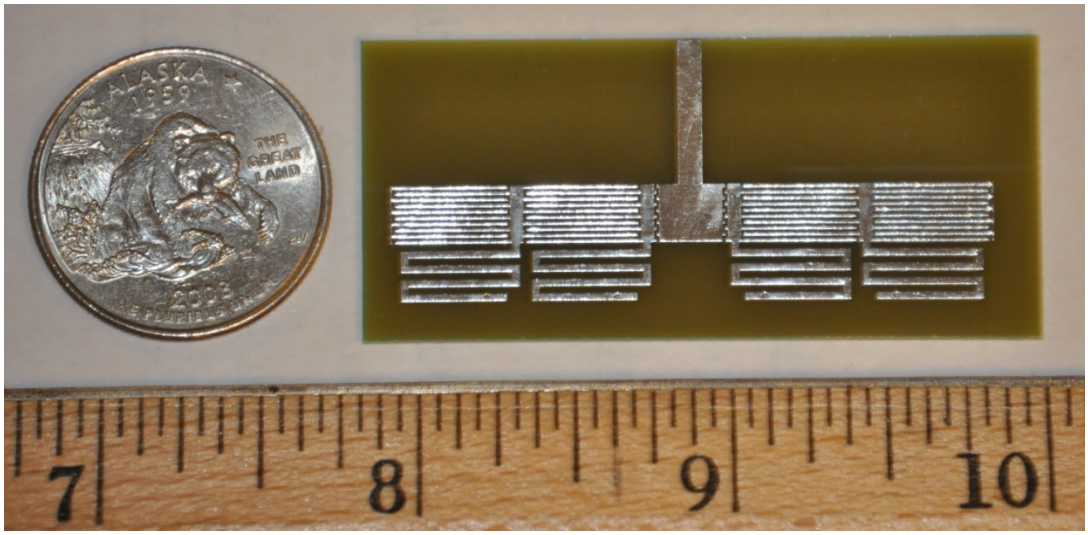

Figure 4-31 Photograph of AUT2

The S11 of the antenna is measured by connecting it to the VNA and the result is shown in Figure 4-32. It can be seen that the antenna resonates at 950 MHz and has a return loss of -7 dB. The antenna is then tested in the anechoic chamber as in the case of AUT1 and the measured power plots are shown in Figure 4-33.

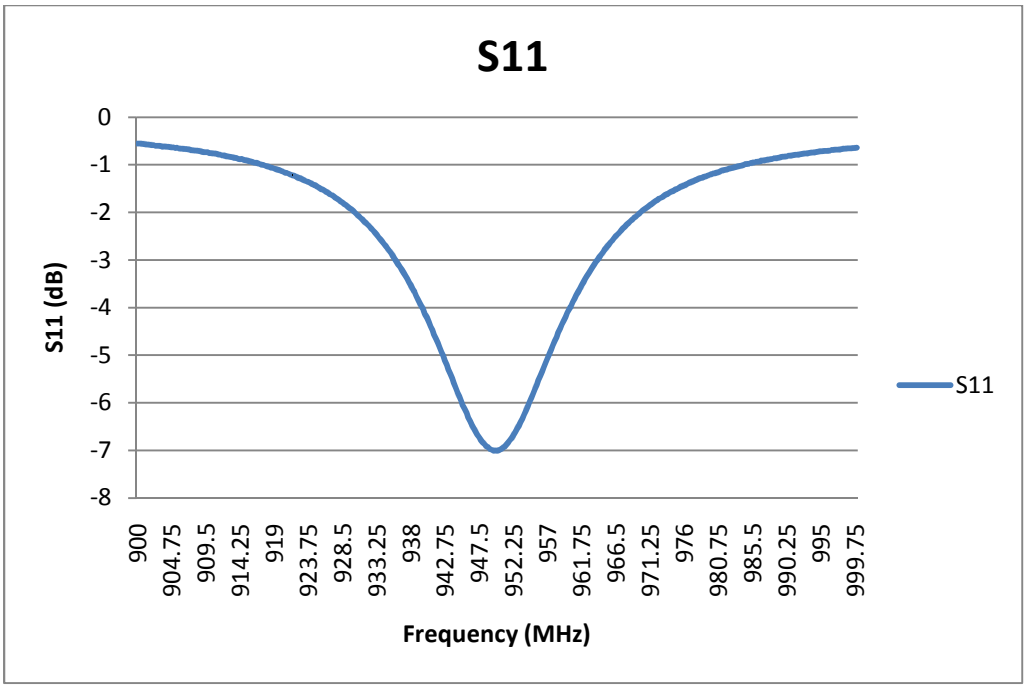

Figure 4-32 Measured S11 - AUT2

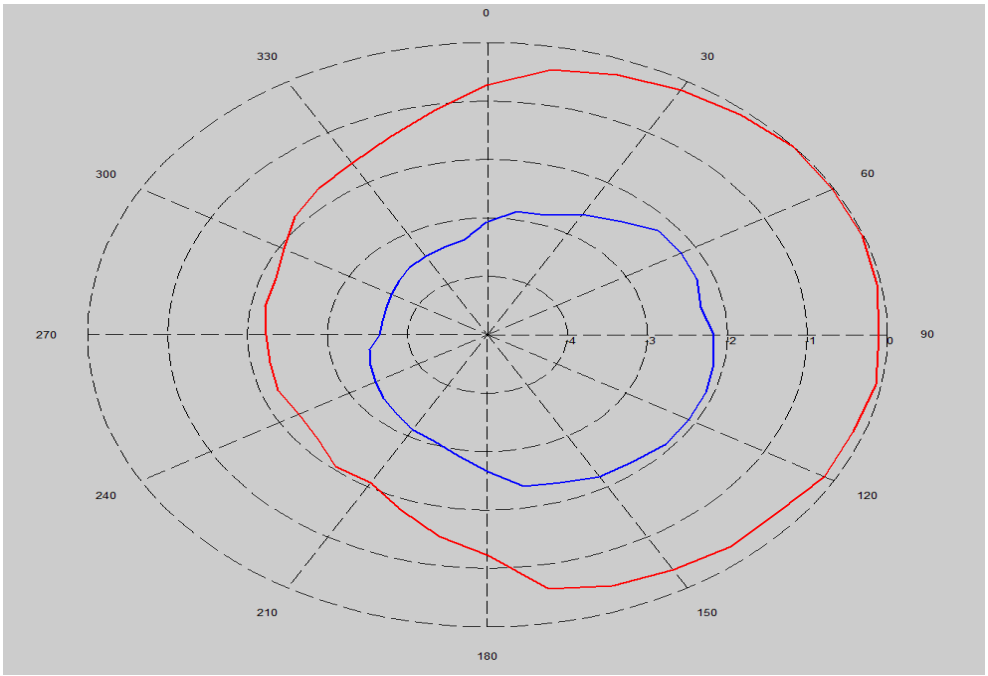

Red: AUT2 parallel to reference

Blue: AUT2 perpendicular to reference

Figure 4-33 Measured power plot – AUT2

4.5.3 AUT3 – Testing Results

The novel CRLH ZOR antenna with 4 cells fed through a strip on top (AUT3) is fabricated on a FR4 substrate. The thickness of the substrate is 1.57mm and the copper thickness is 35 um. A photograph of the fabricated antenna is shown in Figure 4-34.

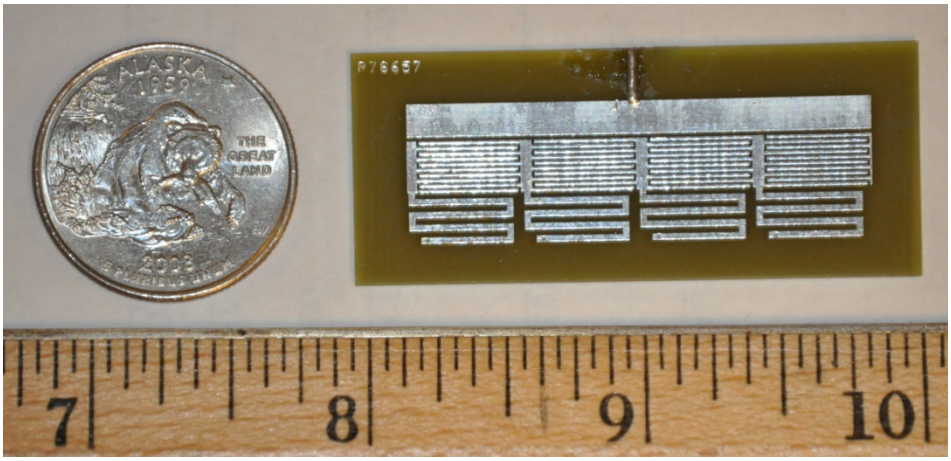

Figure 4-34 Photograph of AUT3

The S11 of the antenna is measured and the plot is shown in Figure 4-35. It can be observed that the antenna resonates at a frequency of 950 MHz and has a return loss of -10 dB.

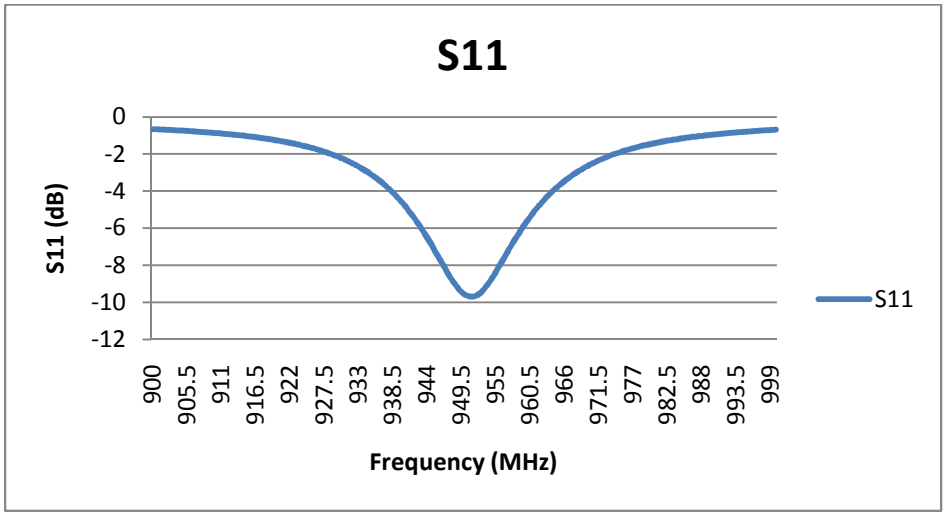

Figure 4-35 Measured S11 – AUT3

The antenna is then tested in the anechoic chamber as in the previous cases and the measured power plots are shown in Figure 4-36.

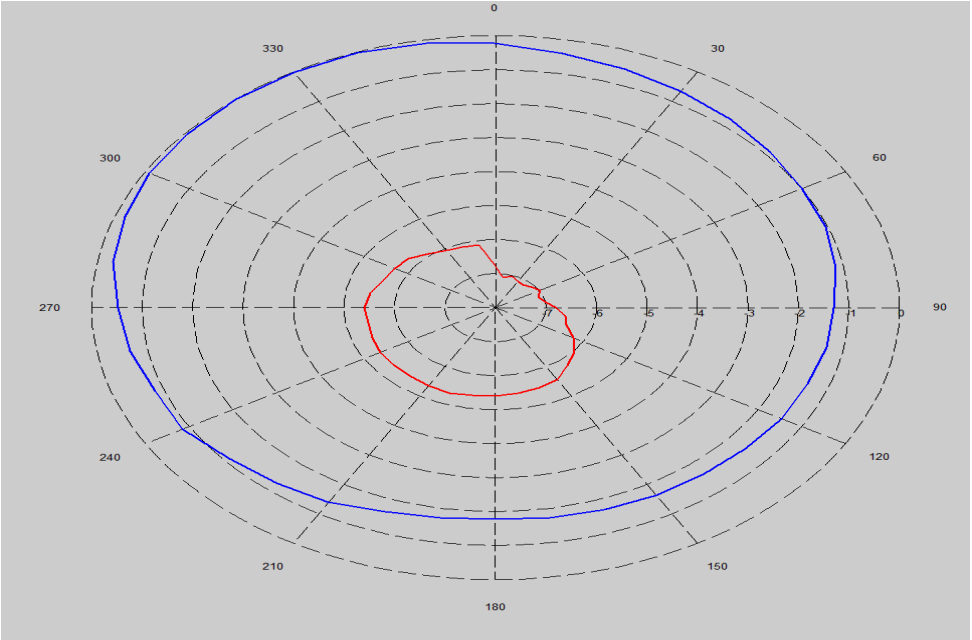

Red: AUT2 parallel to reference

Blue: AUT2 perpendicular to reference

Figure 4-36 Measured power plot – AUT3

It can be observed from the measured results in all three cases that the frequency of resonance has shifted by about 20 MHz from the simulated design. It is also evident that the radiation characteristics of the antennas are not exactly as predicted by the ADS simulations. This can be attributed to the following reasons:

- The ADS simulations assume an infinite ground plane whereas the ground plane is finite in practice. This leads to a change in the pattern of radiation. It can be seen from Figure 4-37 that

when AUT3 is simulated in HFSS with a finite ground plane the radiation pattern is indeed seen to be a broadside pattern which is in agreement with the experimental results.

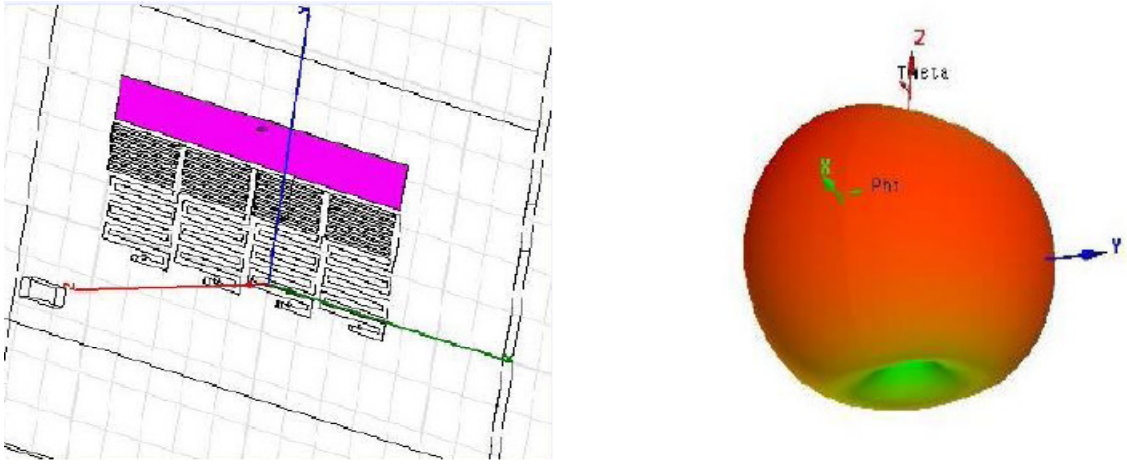

Figure 4-37 HFSS simulation result for AUT3 with finite ground plane

- The small form factor of the antennas makes them very sensitive to fabrication errors. Even a slight error in the etching process can lead to degradation in antenna performance.
- The use of the metal coax connector to connect the antenna to the VNA and the anechoic chamber might cause a difference in the resonant frequency.

4.5.4 Size comparison with a Rectangular Patch Antenna

The simple rectangular patch antenna radiating around the same frequency is also fabricated in order to compare the antenna sizes. The photograph in Figure 4-38 shows the three novel CRLH ZOR antennas placed next to a single rectangular patch antenna.

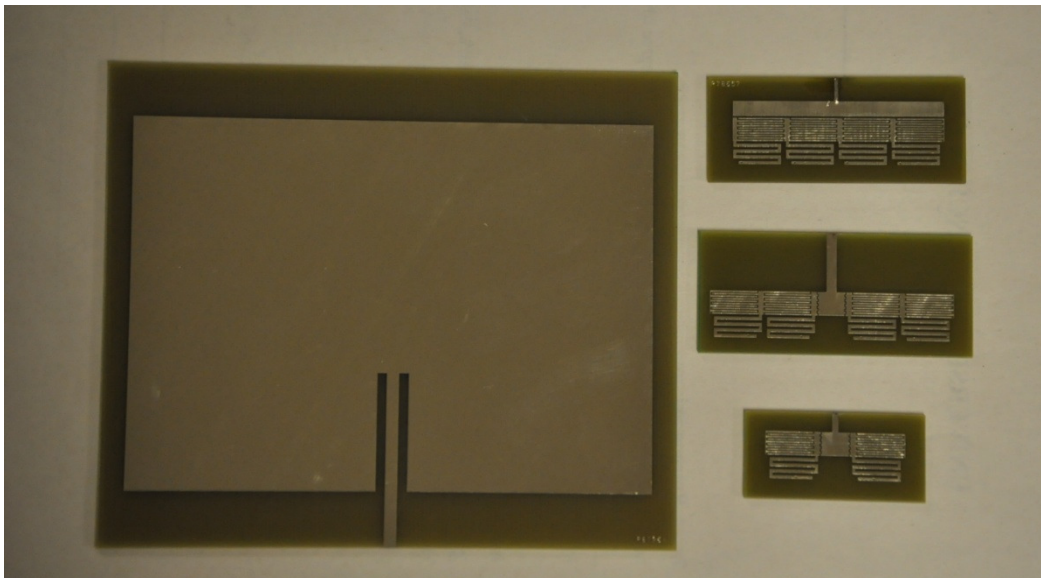

Figure 4-38 Size comparison of rectangular patch and the novel CRLH ZOR antennas

It is clearly visible that the novel CRLH ZOR antennas achieve a significant reduction in size when compared to the rectangular patch antenna. Hence an RFID tag made using the novel CRLH antennas would be the preferred choice rather than a patch antenna RFID tag.

Chapter 5

Summary and Recommendations for Future Work

5.1 Summary

The significant increase in the number of applications with a constraint on component size has made metamaterials a prime topic of research. The major impact of these materials, which are not readily available in nature, lies in the decrease in the component size that can be achieved with proper design. An important microwave application of metamaterials is the Zeroth Order Resonator (ZOR) wherein resonance is achieved at the zeroth mode, which is not possible with traditional materials. The zeroth order resonance implies that the resonance is independent of the physical length of the resonator which makes is theoretically possible to design physically small resonators. This is the concept that has been used to design the ZOR antenna which has a much smaller size when compared to traditional microstrip antennas.

In this thesis the use of metamaterial ZOR antennas for RFID applications has been explored. Three novel configurations (AUT1, AUT2, and AUT3) of the CRLH ZOR antenna radiating in the UHF RFID frequency band were proposed. The novel antennas were simulated using Agilent ADS Momentum and the results were presented and analyzed. The performance of the antennas was compared with that of the traditional CRLH ZOR antennas which were also simulated. The superior performance of the novel configurations was evident from the results shown.

In order to evaluate the performance of the novel antennas, a simple rectangular patch antenna resonating at the same frequency was simulated and the results were compared. Although the performance of the patch antenna was seen to be slightly better, a tremendous reduction in the size of the antenna was achieved in the novel antenna configurations.

The three novel antennas were also simulated for varying values of substrate height, metal thickness, and dielectric loss tangents. The results were presented and the effect of the variation of these parameters on the antenna performance was analyzed. It was found that an increase in the height of the substrate led to an improved antenna performance but with an increase in the weight of the antenna. It was also observed that the change in metal thickness did not have much of an impact on the antenna performance while the decrease in the loss tangent led to a slight improvement in the performance.

The experimental verification of the novel antennas was then presented. The pictures of the fabricated antennas were shown and the antennas were tested using the Vector Network Analyzer to obtain the S11 parameters. The antennas were also tested inside an anechoic chamber and the results were presented. A simple rectangular patch antenna was also fabricated and its size was compared with that of the novel ZOR antennas.

The reduction in size of the novel antennas compared to the patch antenna is one of the most important motivations behind this research. This makes the novel antennas suitable to be used as short-range RFID tag antennas. The RFID tag antennas that are currently used are mostly printed antennas which face a problem of antenna detuning when placed on metal surfaces. This problem is also overcome by the novel CRLH ZOR antennas as it is known that microstrip antennas, which have a ground plane, work well even when placed on metal surfaces.

5.2 Future Work

There exists a lot of opportunity for research in the field of Metamaterials. The exciting possibilities that are promised by the theory of metamaterials need to be physically realized. In this thesis novel CRLH ZOR antennas based on metamaterials were proposed to be used as RFID tag antennas. Although the antenna was simulated and experimentally verified, the

immediate extension of this work would be the actual creation of UHF RFID tags using these antennas. This would require the attachment of a RFID chip to the antennas and a UHF RFID reader to test the tags.

The CRLH ZOR antennas have been found to provide even better results at higher frequencies. Their use at frequencies such as the 1.575 GHz GPS frequency needs to be explored further. It is also important that the radiation characteristics of the ZOR antennas can be understood in a better manner through finite-time domain analysis. This would lead to more efficient antenna designs with beams tailored for specific applications.

There has been some research done on CRLH ZOR antenna arrays such as [79]. The performance improvements provided by an array of CRLH ZOR antennas seems promising and needs to be explored further. The novel antennas proposed in this thesis can also be extended to work as antenna arrays and the performances can be investigated.

The most important constraint for modern-day applications is the size of the components. As further research in the field of metamaterials is performed and smaller components are realized, a lot of potential exists for these components to replace the bigger components currently used. The creation of exciting new applications is also in the offing.

References

[1] V. D. Hunt, A. Puglia, and M. Puglia, *RFID: A Guide to Radio Frequency Identification*, Wiley, New Jersey, 2007.

[2] K. V. S. Rao, P. V. Nikitin, and S. F. Lam, "Antenna design for UHF RFID tags: A review and a practical application", *IEEE Transactions on Antennas and Propagation*, vol. 53, no. 12, pp. 3870-3876, Dec 2005.

[3] S. Y. Chen and P. Hsu, "CPW-fed folded-slot antenna for 5.8 GHz RFID tags", *Electron. Lett*., vol. 24, pp. 1516-1517, Nov 2004.

[4] S. K. Padhi, N. C. Karmakar, C. L. Law, and S. Aditya, "A dual polarized aperture coupled circular patch antenna using a C-shaped coupling slot", *IEEE Transactions on Antennas and Propagation,* vol. 51, no. 12, pp. 3295-3298, Dec 2003.

[5] G. Marrocco, "Gain-optimized self-resonant meander line antennas for RFID applications", *IEEE Trans. Antennas Propag. Lett.*, vol. 2, no. 21, pp. 302-305, 2003.

[6] M. Hirvonen, P. Pursula, K. Jaakkola, and K. Laukkanen, "Planar inverted-F antenna for radio frequency identification", *Electron. Lett.*, vol. 40, pp. 848-850, Jul 2004.

[7] Q. Xianming and Y. Ning, "A folded dipole antenna for RFID", *Proc. IEEE Antennas and Propagation Soc. Int. Symp.*, vol. 1, pp. 97-100, Jun 2004.

[8] Ng et al, "RFID tags for metallic object identification", RFID Handbook: Applications, Technology, Security, and Privacy, CRC Press, Mar 2008.

[9] P. R. Foster and R. A. Burberry, "Antenna problems in RFID systems", *RFID Technology (Ref. No. 1999/123), IEE Colloquium*, pp. 3/1-3/5, Oct 1999.

[10] J. T. Prothro, G. D. Durgin, and J. D. Griffin, "The effects of a metal ground plane on RFID tag antennas", *Proc. IEEE Antennas and Propagation Soc. Int. Symp.*, pp. 3241-3244, Jul 2006.

[11] P. Raumonen et. al., "Folded dipole antenna near metal plate", *Antennas and Propagation Soc. Int. Symp.*, vol. 1, pp. 848-851.

[12] D. M. Dobkin and S. M. Weigand, "Environmental effects on RFID tag antennas", IEEE Microwave Symposium Digest, pp. 135-138, Jun 2005.

[13] J. D. Griffin, G. Durgin, A. Haldi, and B. Kippelen, "Radio link budgets for 915 MHz RFID antennas placed on various objects", *WCNG Wireless Symposium*, Oct 2005.

[14] J. Prothro, "Improved performance of a radio frequency identification tag antenna on a metal ground plane", Master of Science Thesis, Georgia Institute of Technology, 2007.

[15] V. Veselago, "The electrodynamics of substances with simultaneous negative values of ε and μ", *Soviet Physics Uspekhi*, vol. 10, no. 4, pp. 509-514, Jan., Feb. 1968.

[16] D. R. Smith, W. J. Padilla, D. C. Vier, S. C. Nemat-Nasser, and S. Schultz, "Composite medium with simultaneously negative permeability and permittivity", *Phys. Rev. Lett.*, vol. 84, no. 18, pp. 4184-4187, May 2000.

[17] C. Caloz and T. Itoh, *Electromagnetic Metamaterials: Transmission Line Theory and Microwave Applications*, New York: Wiley, 2004.

[18] B. Zhao, "Composite right/left-handed (CRLH) Microstrip resonant antennas", Master of Science Thesis, University of Cincinnati, 2005.

[19] J. C. Maxwell, *A Treatise on Electricity and Magnetism*, Oxford University Press, London, UK, 1873, 1904.

[20] H. R. Hertz, *Electric Waves*, London: McMillian, 1893; New York, Dover, 1962.

[21] J. D. Kraus, "Antennas since Hertz and Marconi", *IEEE Trans. Antennas and Propagat.*, vol. AP-33, pp. 131-137, Feb. 1985.

[22] S. Silver, *Microwave Antenna Theory and Design*, MIT Radiation Lab. Series, vol. 12, New York: McGraw-Hill, 1949.

[23] C. G. Christodoulou and P. F. Wahid, *Fundamentals of Antennas: Concepts and Applications*, SPIE-The International Society for Optical Engineering, 2001.

[24] A. W. Rudge, K. Milne, A. D. Olver, and P. Knight (Eds.), *The Handbook of Antenna Design*, Vols. 1 and 2, Peter Peregrinus, London, 1982.

[25] W. L. Stutzman and G. A. Thiele, *Antenna Theory and Design*, Wiley, 1998.

[26] C. A. Balanis, *Antenna Theory: Analysis and Design*, Wiley, 2005.

[27] "IEEE Standard Definitions of Terms for Antennas", IEEE Std. 145-1983, *IEEE Trans. Antenna Propagat.*, vol. AP-31, pt. II, 1983. Revised IEEE Std. 145-1993.

[28] G. A. Deschamps, "Microstrip Microwave Antennas", Presented at the Third USAF Symposium on Antennas, 1953.

[29] H. Gutton and G. Baissinot, "Flat aerial for Ultra High Frequencies", French Patent No. 703 113, 1955.

[30] R. E. Munson, "Single slot cavity antennas assembly", U.S. Patent No. 3713 162, Jan. 1973.

[31] R. E. Munson, "Conformal microstrip antennas and microstrip phased arrays", *IEEE Trans. Antenna Propagat.*, vol. AP-22, no. 1, pp. 74-78, Jan. 1974.

[32] D. M. Pozar, "A review of bandwidth enhancement techniques for microstrip antennas", *Ch.4* in Microstrip Antennas, ed. D. M. Pozar and D. H. Schaubert, IEEE Press, 1995.

[33] H.F. Pues and A. R. Van de Capelle, “An impedance-matching technique for increasing the bandwidth of microstrip antennas”, *Ch.4* in Microstrip Antennas, ed. D. M. Pozar and D. H. Schaubert, IEEE Press, 1995.

[34] P. S. Hall, “Probe compensation in thick microstrip patches”, *Ch.4* in Microstrip Antennas, ed. D. M. Pozar and D. H. Schaubert, IEEE Press, 1995.

[35] D. M. Pozar and B. Kaufman, “Increasing the bandwidth of a microstrip antenna by proximity coupling”, *Ch.4* in Microstrip Antennas, ed. D. M. Pozar and D. H. Schaubert, IEEE Press, 1995.

[36] K. R. Carver and J. W. Mink, “Microstrip antenna technology”, *Ch.1* in Microstrip Antennas, ed. D. M. Pozar and D. H. Schaubert, IEEE Press, 1995.

[37] G. R. Traut, “Clad laminates of PTFE composites for microwave antennas”, *Microwave Journal*, vol. 23, no. 11, pp. 47-51, Nov. 1980.

[38] M. Olyphant Jr. and T. E. Nowicki, “Microwave substrates support MIC technology”, *Microwaves*, part I, vol. 19, no. 12, pp. 74-80, Nov. 1980.

[39] K. F. Lee and K. M. Luk, *Microstrip Patch Antennas*, Imperial College Press, 2011.

[40] E. H. Van Lil and A. R. Van de Capelle, “Transmission-line model for mutual coupling between microstrip antennas”, *IEEE Trans. Antenna Propagat.*, vol. AP-32, no. 8, pp. 816-821, Aug. 1984.

[41] A. G. Derneryd, “A theoretical investigation of the rectangular microstrip antenna element”, *IEEE Trans. Antenna Propagat.*, vol. AP-26, no. 4, pp. 532-535, Jul. 1978.

[42] K. Malkomes, “Mutual coupling between microstrip patch antennas”, *Electronic Letters*, vol. 18, no. 122, pp. 520-522, Jun. 1982.

[43] E. Penard and J. P. Daniel, "Mutual coupling between microstrip antennas", *Electronic Letters*, vol. 18, no. 4, pp. 605-607, Jul. 1982.

[44] C. A. Balanis, *Advanced Engineering Electromagnetics*, John Wiley & Sons, New York, 1989.

[45] E. O. Hammerstad, "Equations for microstrip circuit design", *Proc. Fifth European Microwave Conf.*, pp. 268-272, Sep. 1975.

[46] G. Kumar and K. P. Ray, *Broadband Microstrip Antennas*, Artech House, 2003.

[47] J. D. Jackson, *Classical Electrodynamics*, Wiley, New York, 1999.

[48] L. D.Landau, E. M. Lifshitz, and L. P. Pitaevskii, *Electrodynamics of Continuous Media*, Pergamon, New York, 1984.

[49] V. G. Veselago, "Formulating Fermat's principle for light travelling in negative refraction materials", *Physics – Uspekhi*, vol. 45, pp. 1097-1099, 2002.

[50] I. V. Lindell, S. A. Tretyakov, K. I. Nikoskinen, and S. Ilvonen, "BW-media with negative parameters, capable of supporting backward waves", *Microwave Opt. Tech. Lett.*, vol. 31, pp. 129-133, 2001.

[51] R. W. Ziolkowski and E. Heynman, "Wave propagation in media having negative permeability and permittivity", *Phys. Rev. E*, vol. 64, paper 056625, 2001.

[52] J. B. Pendry, A. J. Holden, W. J. Stewart, and I. Youngs, "Extremely low frequency plasmons in metallic mesostructure", *Phys. Rev. Lett.*, vol. 76, no. 25, pp. 4773-4776, Jun. 1996.

[53] J. B. Pendry, A. J. Holden, D. J. Robbins, and W. J. Stewart, "Low frequency plasmons in thin-wire structures", *J. Phys. Condens. Matter*, vol. 10, pp. 4785-4809, 1998.

[54] R. A. Shelby, D. R. Smith, and S. Schultz, "Experimental verification of a negative index of refraction", *Science*, vol. 292, pp. 77-79, Apr. 2001.

[55] P. Markos and C. M. Soukoulis, "Numerical studies of left-handed materials and arrays of split ring resonators", *Phys. Rev. E*, vol. 65, pp. 036622:1-8, 2002.

[56] P. Markos and C. M. Soukoulis, "Transmission studies of left-handed materials", *Phys. Rev. B*, vol. 65, pp. 033401:1-4, 2002.

[57] R. W. Ziolkowski, "Pulsed and CW Gaussian beam interactions with double negative metamaterial slabs", *Optics Express*, vol. 11, no. 7, pp. 662-681, Apr. 2003.

[58] C. Caloz, C. C. Chang, and T. Itoh, "Full-wave verification of the fundamental properties of left-handed materials (LHMs) in waveguide configurations", *J. App. Phys.*, vol. 90, no. 11, pp. 5483-5486, Dec. 2001.

[59] P. P. M. So and W. J. R. Hoefer, "Time domain TLM modeling of metamaterials with negative refractive index", *IEEE-MTT Int'l Symp.*, pp. 1779-1782, Fort Worth, TX, Jun. 2004.

[60] J. A. Kong, B. I. Wu, and Y. Zhang, "A unique lateral displacement of a Gaussian beam transmitted through a slab with negative permittivity and permeability", *Micr. Opt. Technol. Lett.*, vol. 33, no. 2, pp. 136-139, Apr. 2002.

[61] D. R. Smith, D. Schurig, and J. B. Pendry, "Negative refraction of modulated electromagnetic waves", *App. Phys. Lett.*, vol. 81, no. 15, pp. 2713-2715, Oct. 2002.

[62] M. W. McCall, A. Lakhtakia, and W. S. Weiglhofer, "The negative index of refraction demystified", *Eur. J. Phys.*, vol. 23, pp. 353-359, 2002.

[63] A. K. Iyer and G. V. Eleftheriades, "Negative refractive index metamaterials supporting 2-D waves", *in IEEE-MTT Int'l Symp.*, vol. 2, pp. 412-415, Seattle, WA, Jun. 2002.

[64] C. Caloz and T. Itoh, "Transmission line approach of left-handed (LH) structures and microstrip realization of a low-loss broadband LH filter", *IEEE Trans. Antennas Propagat.*, vol. 52, no. 5, pp. 1159-1166, May. 2004.

[65] R. W. Ziolkowski, "Design, fabrication, and testing of double negative metamaterials", *IEEE Trans. Antennas Propagat.*, vol. 51, no. 7, pp. 1516-1529, Jul. 2003.

[66] A. Sanada, C. Caloz, and T. Itoh, "Planar distributed structures with negative refractive index", IEEE Trans. Microwave Theory Tech., vol. 52, no. 4, pp. 1252-1263, Apr. 2004.

[67] S. H. Lee, C. M. Park, Y. M. Seo, and C. K. Kim, "Reversed Doppler effect in double negative metamaterials", Phys. Rev. B., vol. 81, pp. 241102:1-4, 2010.

[68] A. Grbic and G. V. Eleftheriades, "A backward-wave antenna based on negative refractive index L-C networks", *Proc. IEEE-AP-S USNC/URSI National Radio Science Meeting*, vol. 4, San Antonio, TX, pp. 340-343, Jun. 2002.

[69] A. A. Oliner, "A periodic-structure negative-refractive-index medium without resonant elements", URSI Digest, *IEEE-AP-S USNC/URSI National Radio Science Meeting*, vol. 4, San Antonio, TX, pp. 41, Jun. 2002.

[70] C. Caloz and T. Itoh, "Application of the transmission line theory of left-handed (LH) materials to the realization of a microstrip LH transmission line", *Proc. IEEE-AP-S USNC/URSI National Radio Science Meeting*, vol. 2, San Antonio, TX, pp. 412-415, Jun. 2002.

[71] C. Caloz, H. Okabe, T. Iwai, and T. Itoh, "Anisotropic PBG surface and its transmission line model", *URSI Digest*, *IEEE-AP-S USNC/URSI National Radio Science Meeting*, pp. 224, San Antonio, TX, Jun. 2002.

[72] A. Lai, C. Caloz, and T. Itoh, "Composite right/left handed transmission line metamaterials", *IEEE Microwave Magazine*, vol. 5, no. 3, pp. 34-50, Sep. 2004.

[73] C. Caloz and T. Itoh, "Novel microwave devices and structures based on the transmission line approach of meta-materials", *IEEE-MTT Int'l Symp.*, vol. 1, pp. 195-198, Philadelphia, PA, Jun. 2003.

[74] A. Sanada, C. Caloz, and T. Itoh, "Characteristics of the composite right/left-handed transmission lines", *IEEE Microwave Wireless Compon. Lett.*, vol. 14, no. 2, pp. 68-70, Feb. 2004.

[75] C. Caloz, H. Okabe, T. Iwai, and T. Itoh, "Transmission line approach of left-handed (LH) materials", *USNC/URSI National Radio Science Meeting*, vol. 1, pp. 39, San Antonio, TX, Jun. 2002.

[76] R. Shi, "Zeroth-Order Resonator (ZOR) antenna using Composite Right/Left-Handed Microstrip Transmission Line ", Master of Science Thesis, University of Cincinnati, 2011.

[77] J. R. Aguilar, M. Beadle, P. T. Thompson, and M. W. Shelley, "The microwave and RF characteristics of FR4 substrates", *Digest Inst. Elect. Eng. Colloq. On Low Cost Antenna Technology (1998/206)*, pp. 2/1-2/6, London, UK, Feb 1998.

[78] http://edocs.soco.agilent.com/display/ads2008U2/MICAP1+(Microstrip+Interdigital+Capacitor+(2-port))

[79] A. A. Fashi, M. Kamyab, and M. Barati, "A novel small resonant antenna using the meta-materials array", *PIERS Proceedings*, pp. 670-674, Moscow, Russia, Aug 2009.